OPTICAL AND ELECTRONIC PROPERTIES OF HYDROGENATED AMORPHOUS $Si_{1-X}Ge_X$ ALLOYS

by

R.D. McLeod

A thesis
presented to the University of Manitoba
in partial fulfillment of the
requirements for the degree of
Master of Science
in
Electrical Engineering

Winnipeg, Manitoba, 1982

OPTICAL AND ELECTRONIC PROPERTIES

OF

HYDROGENATED

AMORPHOUS $Si_{1-x}Ge_x$ ALLOYS

BY

ROBERT D. MCLEOD

A thesis submitted to the Faculty of Graduate Studies of
the University of Manitoba in partial fulfillment of the requirements
of the degree of

MASTER OF SCIENCE

The University of Manitoba requires the signatures of all persons using or photocopying this thesis. Please sign below, and give address and date.

ABSTRACT

The optical properties of amorphous hydrogenated $Si_{1-x}Ge_x$ thin films, prepared by the radio frequency sputtering technique have been measured over the range of composition $0.0 \leq x \leq 1.0$ at wavelengths of $0.35\mu m \leq \lambda \leq 2.65\mu m$, by spectrophotometry and ellipsometry. Both the index of refraction (n) and the extinction coefficient (k) were observed to be dispersive over this range of λ. In general two peaks in n were observed, with one peak believed to be below the optical absorption edge, while k exhibits at least one peak, with structure at the longer wavelengths. The photon energy at these peaks is dependent upon the composition (x) of the a:$Si_{1-x}Ge_x$(H) material through approximatly linear relationships.

On the basis of the data for n and k, the real and imaginary parts of the dielectric constant, and the absorption coefficient (α) of these films have been determined. An interpretation of the dielectric constant is presented in terms of the exciton-like behavior of bound electron-hole pairs and carrier-trap pairs. The optical absorption coefficient exhibits a tail structure indicative of localized states near the band edges. Assuming a parabolic density of states within the bands, the optical gap (E_{opt}) has been

extracted. The dependence of E_{opt} upon composition x was observed, with $E_{opt} \simeq 1.5$ eV for a:Si(H) decreasing linearly to $E_{opt} \simeq 0.7$ eV for a:Ge(H).

The electronic properties of these materials (dark conductivity and photoconductivity) have also been measured employing phase-sensitive detection techniques, as functions of temperature (T), wavelength (λ), optical flux density (F_o), and composition (x). From the temperature dependence of the dark conductivity, the activation energy was determined and found to decrease monotonically with increasing x. The photoconductivity was found to be proportional to F_o at low intensities (monomolecular recombination) and to $F_o^{1/2}$ at high intensity (bimolecular recombination). A well defined activation energy of about 0.35 eV was obtained from the temperature dependence of the photoconductivity at $\lambda = 0.6328$ μm, for small values of x. The optical gap was extracted from the spectral dependence of the photoconductivity, and corresponded well with that obtained from the optical measurements. An interpretation of the electronic density of states is advanced on the basis of a modified Davis-Mott model for the density of states in this material.

ACKNOWLEDGEMENTS

The author wishes to thank Prof. H.C. Card for his patient supervision and encouragement throughout the extent of this project.

The author also wishes to extend his thanks to Prof. K.C. Kao for his assistance and discussions. The author is also indebted to his colleagues at the Material and Devices Research Lab., in particular Gord M^{c}Gonigal, Doug Thomson, Doug Buchannan and Sergio Mejia.

Financial support from the Natural Sciences and Engineering Research Council of Canada is gratefully acknowledged.

Special thanks to Sandra.

INTRODUCTION

The optical and electrical properties of amorphous silicon, germanium and silicon-germanium alloy thin films are of considerable interest in the diagnosis of the energy distribution of electronic states in these materials. This in turn relates directly to the suitability of the films for photovoltaic applications, in particular for potential low-cost solar cells.

Over the past decade considerable improvement in amorphous (Si) semiconductor devices has been achieved, primarily due to the discovery of doping control [20]. The most important difficulty to overcome was the high density of states in the gap produced by natural defects. The high density of gap states pinned the Fermi level, thereby making doping difficult if not impossible. The density of these defects, of which the dangling bond was assumed to be the prominent prototype (although not the exclusive cause) was reduced by deposition or annealing at higher temperatures. However the most significant improvement in reducing the density of defect states came from the accidental or fortuitous addition of hydrogen in the preparation of the sample. It was thought hydrogen easily formed covalent Si-H bonds thereby shifting states from deep in the gap into the va-

lence band (saturation of dangling bonds). The reduction in the density of gap states facilitated doping control which subsequently lead to the development of useful semiconductor devices (many of which are in the research phase).

The optical and electronic properties of amorphous silicon (a:Si) and amorphous germanium (a:Ge) films have been extensively investigated and a great deal of experimental information is available for films prepared under a wide variety of fabrication conditions [1-6]. The present study extends the earlier work in several ways: 1) Both the real and imaginary components of the refractive index (n and k) are measured over a wide range of photon energy. This is accomplished using spectrally-resolved ellipsometry which unlike other techniques, allows n to be determined in the high absorption region (where k is large); 2) The composition (x) of the hydrogenated amorphous $Si_{1-x}Ge_x$ thin films is a variable in these experiments; and 3) the photoconductivity is measured as a function of temperature, composition (x), optical intensity and wavelength of excitation, which provides insight into both the electronic structure and probable transport properties.

One of the most interesting and important problems concerning amorphous materials is how and why the electronic structure in non-crystalline form differs from that in crystalline form. A great deal of literature has concentrated on a:Si and a:Ge under various fabrication and experimental

conditions [1-13]. So far relativly little has been reported about the properties of amorphous silicon-germanium alloys [14]. Beaglehole and Zavetova [15] were the first to report the measurement of the absorption edge of such alloy films fabricated by vacuum evaporation. They found that the absorption edge and characteristics of the broad absorption band varied linearly with alloy composition. Later, Chevallier et al. [16] reported that the optical band gap of hydrogenated a:Si-Ge alloy films prepared by radio frequency glow discharge also varies linearly with the alloy composition.

One of the earlier studies of the photoconductivity of a:Si(H) were those by Spear et al.[22,23], which were made in conjunction with field effect measurements in order to deduce an appropriate model for the density of states. More recently optically induced conductivity changes have been studied by Stabler and Wronski [34], to determine the effect of prolonged optical exposure on the photoconductivity. One of the most recent studies by Dong et al.[19] involves the systematic study of the electrical properties of a:$Si_{1-x}Ge_x$(H) thin films. Their studies indicate that films with $0.18 \leq x \leq 0.25$ may prove to be most important in terms of photovoltaic energy conversion.

This study presents systematic data concerning the optical and electrical properties of hydrogenated amorphous $Si_{1-x}Ge_x$ alloys. The hydrogenated amorphous $Si_{1-x}Ge_x$ films

were deposited onto glass substrates by radio frequency (r.f.) sputtering in a sputtering gas containing Ar with either 5% or 25% H_2. An interpretation of the electronic density of states is advanced in terms of a modified Davis-Mott model [1].

Chapter 1 presents an overview of amorphous materials with emphasis on silicon-like materials, including background material necessary to describe electrical and optical phenomena. Chapter 2 presents and discusses results obtained from the optical measurements of n and k on a:Si_{1-x} Ge_x(H) thin films. Chapter 3 presents and discusses the results obtained from the electrical measurments. Chapter 4 presents the conclusions deduced from the optical and electrical measurements.

CONTENTS

ABSTRACT	iii
INTRODUCTION	vi
Chapter	page
I. AN OVERVIEW OF THE AMORPHOUS SEMICONDUCTORS	1
The Amorphous State	1
The Density of States	2
The Crystalline Case	2
Anderson Localization and the Amorphous State	3
Models	5
The Davis-Mott Model	5
Electrical Transport	7
Conduction in Extended States	7
Conduction in the Band Tails	9
Nearest Neighbor Hopping in the Band Tails	9
Variable Range Hopping in a Tail of localized States	12
Conduction in Localized States at the Fermi Level	15
Conductivity Summary	17
Drift Mobility and Photoconductivity	18
Drift Mobility and the effect of Traps	18
Photoconductivity	19
Spectral Dependence of the Photoconductivity	20
Temperature Dependence of the Photoconducivity	21
Photoconductivity and Recombination	27
Optical Absorption	28
The Imaginary Part of the Dielectric Constant ε''	29
The Absorption Coefficient	32
II. DISPERSION OF THE OPTICAL CONSTANTS OF a:$Si_{1-x}Ge_x$(H)	36
Experimental Techniques	36
Experimental Results	40
Discussion	50
III. ELECTRONIC PROPERTIES OF a:$Si_{1-x}Ge_x$(H) THIN FILMS	61
Experimental Techniques	61
Results and Discussion	62
IV. CONCLUSIONS	72
REFERENCES	76

LIST OF FIGURES

Figure		Page
1.1	Schematic representation of the localized tail states	12
1.2	Illustration of $\ln\sigma$ vs. T^{-1} indicating the various modes of conduction	18
1.3	Photocurrent in a:Si plotted against inverse temperature. Spear et al. [20-24]	22
1.4	Schematic energy level diagram including the main features of the density states for a:Si	23
1.5	ε'' for a:Ge as determined by Donovan and Spicer [39]	31
2.1	The real part of the refractive index n for $a:Si_{1-x}Ge_x(H)$ thin films	40
2.2	The imaginary part of the refractive index k for $a:Si_{1-x}Ge_x(H)$ thin films	41
2.3	n_p and E_p as functions of composition	43
2.4	n and k at a fixed photon energy (2.6 eV) as functions of compositions	43
2.5	Real part of the dielectric constant as a function of photon energy	44
2.6	Imaginary part of the dielectric constant as a function of photon energy	45
2.7	Absorption coefficient as a function of photon energy	46
2.8	α at a fixed photon energy of 1.96eV, and the photon energy $\hbar\omega$ for a fixed value of α as functions of x	47

2.9 $(\alpha\hbar\omega)^{1/2}$ as a function of photon energy $\hbar\omega$ 49

2.10 E_{opt} as a function of composition x 49

3.1 Dark-current as a function of inverse temperature 63

3.2 Photocurrent as a function of inverse temperature 63

3.3 Photocurrent as a function of illumination intensity 65

3.4 Photocurrent as a function of the electric field 66

3.5 Photocurrent as a function of inverse temperature 67

3.6 Spectral dependence of the photocurrent 67

3.7 $(I_{ph}\hbar\omega/eF_o(1-R))^{1/2}$ versus $\hbar\omega$ 69

3.8 E_{opt} as a function of composition x 69

4.1 Schematic representation of the density of states 74

Chapter I

AN OVERVIEW OF AMORPHOUS SEMICONDUCTORS

1.1 THE AMORPHOUS STATE

Amorphous semiconductors are characterized by the repetition of one or more basic molecular units without the structure associated with any infinite periodic array. That is amorphous materials lack long range order of constituent atoms, but they are not completely disordered on the atomic scale either. There exists strong correlation ordering up to third or forth nearest neighbors with respect to bond angle and bond length. It is this lack of long range order together with the maintained short range order which gives the amorphous solid many of its interesting characteristics. It is the short range order that is responsible for optical absorption edges and activated electrical conductivities.

Many amorphous solids are a combination of fully coordinated and defective amorphous states. For example amorphous silicon or germanium generally display fourfold (tetrahedral) coordination as in the crystal; the contribution to the defective amorphous state mainly arises from the preparation technique. A great deal of research is being done relating the structural features to the optical and electrical properties.

Nearest neighbor bond length and bond angle fluctuations give rise to strong electronic scattering and short coherence length of wave functions. Under these circumstances the momentum selection rule breaks down, creating one of the most important differences between the crystalline and amorphous phases.

In many of the fully coordinated amorphous solids the preservation of short range order is responsible for an "energy gap", somewhat similar to their crystalline counterparts. Near the band edges fluctuations in atomic configuration are accompanied by fluctuations in potential seen by an electron. These fluctuations are responsible for band-tails of localized states. Transitions between localized states are allowed only to the extent that there is spatial overlap of the localized wave functions, whereas transitions between localized and delocalized states beyond the mobility edges are strongly allowed [17].

Properties of fully coordinated amorphous solids are modified when defective materials are considered.

1.2 THE DENSITY OF STATES

1.2.1 The Crystalline Case

In the perfect crystal the potential is perfectly periodic, and as a consequence of the Bloch theorem the one electron wave functions are of the form

$$\psi(r) = \psi_{kn}(r) = e^{ikr} U_{kn}(r) \qquad (1.1)$$

The wave vector k is in the first Brillouin zone. $U_{kn}(r)$ has the periodicity of the crystal, and n is the band index. The magnitude of ψ is of the same order everywhere and the long range phase coherence is retained. Thus all wave functions are "extended". These are the eigenfunctions of Schroginger's wave equation with corresponding eigenvalues $E=E_n(k)$. These eigenvalues are the electron energies which fall into quasi-continuous bands (in the limit of large numbers of atoms) of allowed energy separated by forbidden gaps. The density of states also exhibit $E^{1/2}$ dependence, with singularities at the band edges.

The extended nature of the states and the sharp band edges are a direct consequence of the perfect translational order of the crystal.

1.2.2 Anderson Localization and the Amorphous State

When sufficient disorder exists, but short range order is maintained, there exist solutions to Schrodinger's wave equation which are not extended but are localized in space. This was proved by Anderson [18] in 1958. The wave functions corresponding to localized states are of the form

$$\psi(r) = \psi_{kn}(r)\exp(-\alpha r) \qquad (1.2)$$

Where α is defined such that $\exp(-\alpha r)$ is the rate at which the wave function decays with distance. Mott and Davis [1] have postulated that localized and extended states cannot co-exist at the same energy.

The separation of localized and extended states occurs at a critical energy Ec (or Ev) and is defined as follows

$$\langle \sigma_E \rangle = 0 \ (E<Ec)$$
$$\neq 0 \ (E \geq Ec) \quad @ \quad T = 0K \tag{1.3}$$

where σ_E is the conductivity due to states at energy E. The above definition does not imply a discontinuity in the density of states N(E). For the amorphous semiconductor Ec is referred to as the "mobility edge" after Cohen [19] . If the decay parameter α has the following form [1]

$$\alpha \propto \alpha_o \left(\frac{Ec - E}{Ec} \right)^s \tag{1.4}$$

the wave functions near Ec have strong overlap. When E=Ec, α tends to zero and the states become extended. At this point the conductivity can be calculated and is called the minimum metallic conductivity (σ_{min}). According to Mott and Davis [1], if σ_{min} exists the conductivity σ_E should show a discontinuity at Ec. The minimum metallic conductivity has been shown to be approximatly

$$\sigma_{min} \simeq \frac{0.026e^2}{\hbar a} \tag{1.5}$$

where a is the interatomic spacing.

1.2.3 Models

The density of states remains a valid concept in understanding amorphous materials. With the presence of short range order in amorphous semiconductors the essential features of the crystalline phase are approximatly preserved. Along with retaining these crystalline features, gap states exist as a consequence of defects and due to a lack of long range order.

An early model proposed was the Cohen-Fritzsche-Ovshinsky model [19] in 1969. The C-F-O model consisted of tail states which extended across the gap in a structureless distribution. These tails of localized states could then overlap and pin the Fermi level near the middle of the gap. Another concept introduced at that time was the existence of mobility edges. The mobility edge was defined as the critical energy which separated extended and localized states. The gap between the mobility edges was defined as the mobility gap. There is considerable evidence for the existence of mobility edges but the existence of deep tail states is now considered unlikely in most amorphous semiconductors.

1.2.4 The Davis-Mott Model

The Davis-Mott model is based on the requirements demanded by experimental results, primarily the pinning of the Fermi level at a finite density of states. This finite density of states at E_f was postulated to result from defects in the

atomic network (dangling bonds, voids, bent bonds, vacancies, etc.). The defects give rise to localized states with energies deep in the energy gap, in addition to the band tails which result from the absence of long-range order. In the Davis-Mott model the tails of localized states from the conduction and valence bands extend only a few tenths of an electron volt into the forbidden gap. The energy levels Ec and Ev still define a mobility gap, that is Ec and Ev separate the localized and extended states. Mott has suggested that at the transition from extended to localized states (a transition made abrupt by screening effects) the mobility drops by several orders of magnitude, producing a mobility edge.

A modified Davis-Mott model contains bands of acceptor and donor-like defect states; these bands may contain a wide range of localized state densities, with various degrees of overlap between the states. E_f should lie between the two bands if they do not overlap, or be pinned between them if they do overlap.

Experimental results by Spear et al. [20-24] have shown that there exists a local density of defect related states approximatly 1.2 eV below Ec in r.f. glow discharge produced amorphous silicon. This result was derived from field effect measurements and was corroberated by photoconductivity experiments.

The interpretation of experimental data is deeply related to the density of states. From the Davis-Mott model there exist three processes for conduction. Each type of conduction will dominate in a specific temperature range; this subject will form the next section of the discussion.

1.3 ELECTRICAL TRANSPORT

As mentioned previously the mobility edge is an important concept underlying amorphous semiconductors. The mobility edges separate extended and localized states in the valence and conduction bands (localized states originate due to lack of long range order).

The conduction above and below the mobility edge will be considered for non-degenerate conditions. Non-degeneracy implies, for n-type semiconductors, that the Fermi energy E_f is many kT below the conduction band mobility edge and also below E_A, where E_A is the minimum energy of the tail states. This condition insures that the carrier concentrations at Ec and E_A follow Boltzman statistics.

1.3.1 Conduction in Extended States

Much of the following discussion has been adapted from Mott and Davis [1], Nagels [25] and Mott [26]. If the Fermi level is close enough to the extended states or the temperature is high enough, such that a sufficient number of carriers are in the extended states above Ec (or below Ev in the p-

type case) the conductivity may be expressed as follows (if electron conduction is being considered)

$$\sigma = \int_{Ec}^{\infty} eN(E)\mu(E)\cdot kT\partial f(E)/_{\partial E} dE \qquad (1.6)$$

where N(E) is the density of states with $\mu(E)$ and f(E) being the mobility and Fermi function at energy E. Assuming a constant density of states and a constant mobility Eqn.1.6 reduces to

$$\sigma = eN(Ec)kT\mu_c \exp\left\{\frac{-(Ec - E_f)}{kT}\right\} \qquad (1.7)$$

The number of electrons in extended states is given by

$$n = N(Ec)kT \exp\left[\frac{-(Ec - E_f)}{kT}\right] \qquad (1.8)$$

Assuming N(Ec) to be approximately $\langle N(E)\rangle/3$, Eqn.1.7 can be written as

$$\sigma = \sigma(Ec)\exp\left[\frac{-(Ec - E_f)}{kT}\right] \qquad (1.9)$$

where it follows that

$$\sigma(Ec) = e\langle N(E)\rangle\mu_c kT/3 = \sigma_{min} \qquad (1.10)$$

Mott defined $\sigma(Ec)$ as σ_{min} and denoted this quantity as the minimum metallic conductivity. From Mott's derivation

$$\sigma_{min} \simeq \frac{0.026e^2}{\hbar a} \qquad (1.11)$$

Comparing Eqn.1.11 and 1.10 the mobility may be written as

$$\mu_c \simeq \frac{0.075e}{\hbar a\langle N(E)\rangle kT} \qquad (1.12)$$

If N(E) is written as $1/(a^2 B)$, recalling that a is the interatomic spacing and B is the bandwidth, then

$$\mu_c \simeq \frac{0.075\ e\ a^2 B}{\hbar kT} \tag{1.13}$$

Selecting typical values of B and a, $\mu_c \simeq 10 cm^2/V \cdot s$. This estimated value of μ_c corresponds to a mean free path less than the interatomic spacing. Cohen's [27] derivation, assuming diffusive conduction yields the same temperature dependence. Thus the conductivity can be expressed as

$$\sigma = \sigma_{min} \exp\left(\frac{-(Ec - E_f)}{kT}\right) \tag{1.14}$$

Expressing $Ec-E_f$ as a linear function of temperature

$$Ec - E_f = E(0) - \gamma T \tag{1.15}$$

a plot of $\ln\sigma$ versus $1/T$ yields an activation energy $E(0)$ provided $\ln\sigma$ versus $1/T$ is linear over the temperature range where extended state conduction dominates. The σ intercept will then yield $\sigma_{min} \exp(\gamma/k)$.

1.3.2 Conduction in the Band Tails

1.3.2.1 Nearest Neighbor Hopping in the Band Tails

In the band tails where the wave functions are localized, $\langle\sigma(E)\rangle=0$; this implies that the transport of carriers can only occur by thermally activated (phonon assisted) hopping. If electron conduction is being considered, transport can occur from one localized state to another with the emission

or absorption of a phonon or of multiple phonons. Processes in which the energy of the electron is increased are rate determining. If two sites are at a distance R from each other, and the wavefunctions have a decay parameter α such that $\alpha R \ll 1$ (strong overlap of wave functions, weak localizations), then the probability of electron hopping may be calculated as follows:

The probability (frequency) that an electron jumps from one localized state to another with the absorption of a phonon may be expressed as [25]

$$\nu = \nu_{pH} \exp[-2\alpha R - W/kT] \tag{1.16}$$

where ν_{pH} is the phonon frequency and W is the energy difference between the two states. If $\alpha R \ll 1$, that is if overlap is strong (ν is large), hopping processes to nearest neighbor sites will determine the diffusion coefficient. In this case [1],

$$D = \frac{1}{6} \nu_{pH} R^2 \exp[-2\alpha R - W/kT] \tag{1.17}$$

The mobility can then be obtained from the Einstein relation

$$\mu = \frac{eD}{kT} \tag{1.18}$$

It is then expected that the mobility will be of the form

$$\mu = \frac{1}{6} \nu_{pH} e \frac{R^2}{kT} \exp\left(-\frac{\overline{W}(E)}{kT}\right) \tag{1.19}$$

where $\overline{W}(E)=2\alpha RkT+W\simeq W$ for $\alpha R\ll 1$. For a phonon frequency of $\nu_{pH}=10^{13}\ s^{-1}$ and $W\simeq kT$ the mobility is on the order of $10^{-2}\ cm^2/V\cdot s$ at room temperature. Thus the mobility is seen to drop by 2 orders of magnitude when going from extended to localized states, supporting Mott's argument for the existence of a mobility gap.

The above analysis is based on nearest-neighbor hopping conduction. Mott has postulated that nearest-neighbor fixed range hopping can only occur when the total range of localized tail states is comparable to kT, whereas the extent of the localized tail states is believed to be a few tenths of an electron volt. Also in the above analysis there appears to be a contradiction; namely, nearest-neighbor conduction takes place when $\alpha R>>1$, which implies strong localization, whereas the above analysis assumes weak localization. Mott's treatment of variable-range hopping conduction in the band tails of localized states tends to clear these contradictions up.

1.3.2.2 Variable Range Hopping in a Tail of Localized States

If one assumes an energy dependence for the density of states in the tail of localized states between Ec and E_A of the following form [1]

$$N(E) = C(E - E_A)^n \tag{1.20}$$

the spatial separation a_E between the localized states is given by [1]

$$a_E^3 = \frac{1}{N(E)Vo} \tag{1.21}$$

where V_o characterizes the disorder. In the tail of localized states $a_E > a$, and is shown schematicaly as a function of energy in Fig. 1.1 . The spatial extent of overlap of localized state wave functions will also vary with energy as shown in Fig. 1.1 .

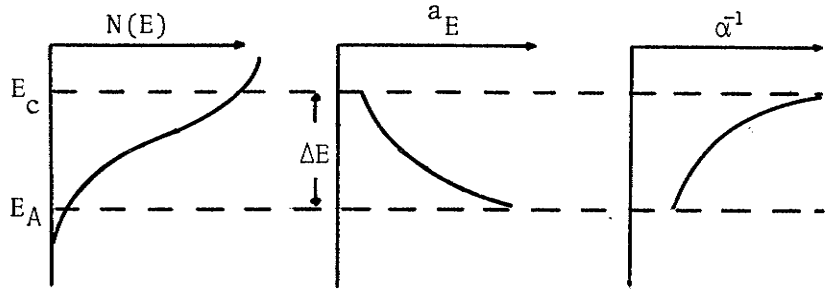

Figure 1.1:a)Density of states N(E) at the edge of the conduction band with a range ΔE of localized states; b)Variation with energy of the average separation between localized states; c)Variation with energy of the decay length α of the localized state wave functions.

Figure 1.1 is drawn such that $\alpha^{-1} \rightarrow \infty$ at E=Ec (states become extended, strong overlapping), and α varies as $(Ec-E)^{s}$, such that α^{-1} is approximatly constant deep in the tail.

According to Mott and Davis [1] and Grant and Davis [28], hopping is considered variable range type; their analysis follows.

The energy Em at which the numbers of carriers is maximum is determined from

$$N(E) = C(E - E_A)^n f(E) \tag{1.22}$$

which yields $Em=E_A+nkT$. The density of states at Em is given by,

$$N(Em) = C(nKT)^n = N(Ec) \left(\frac{nkT}{\Delta E}\right)^n \tag{1.23}$$

where N(Ec) is the density of states at the mobility edge and $\Delta E=Ec-E_A$. Again the hopping probability around Em is written as

$$\nu = \nu_{pH} \exp\left(-2\alpha R - W_1/_{kT}\right) \tag{1.24}$$

where R and W_1 are the variable-range hopping distance and energy. The hopping energy W_1 is written as $3/4\pi R^3 N(Em)$, with N(Em) given by Eqn.1.23. The hopping probability can be maximized to yield the following expressions for R and W_1 [1]

$$R^4 = \frac{9(\Delta E)^n}{8\pi\alpha\, N(Ec) n^n kT^{n+1}} \tag{1.25}$$

$$W_1 = \frac{3}{4}\left(\frac{8}{9}\right)^{\frac{3}{4}} \left\{ \frac{kT^{3-n}\Delta E^n \alpha^3}{n\pi^n N(Ec)} \right\}^{\frac{1}{2}} \qquad (1.26)$$

Therefore the hopping probability will vary as

$$\nu = \nu_{pH} \exp \left\{ 3\left(\frac{8}{9}\right)^{\frac{3}{4}} \frac{\Delta E^n \alpha^3}{\pi N(Ec) n k^{n+1}} \right\}^{\frac{1}{4}} \qquad (1.27)$$

An estimate of the hopping length and energy can be obtained using n=1 (linear tail states), $\Delta E = 0.3$eV, $\alpha^{-1} = 10$ Å, $N(Ec) = 2 \times 10^{21}$ cm^{-3} eV^{-1} and T=300 K. The resulting hopping length and energy are R=30.5 Å and $W_1 = 0.05$ eV. It should be noted that R is considerably larger than a_E, since a_E is approximately 18 Å at an energy 1 kT above E_c.

The relation to the mobility follows from the Einstein relation

$$\mu_{hop} = \frac{eD}{kT} \quad \text{where} \quad D = \frac{1}{6} \nu R^2 \qquad (1.28)$$

Thus $\mu_{hop} = \frac{1}{6} \nu R^2 / kT$ where R is obtained from Eqn.1.25. The mobility in the conduction band tail should have a temperature dependence of the following form

$$\mu_{hop} = C\nu_{pH} T^{\frac{-n+3}{2}} \exp \left\{ - \left(3\left(\frac{8}{9}\right)^{\frac{3}{4}} \left(\frac{\Delta E^n \alpha^3}{\pi N(Ec) n^n k^{n+1}} \right)^{\frac{1}{4}} \right) T^{-\left(\frac{n+1}{4}\right)} \right\} \qquad (1.29)$$

Due to the uncertainty of the temperature dependence of ν_{pH} in the pre-exponential factor of Eqn. 1.29 the magnitude of the mobility is difficult to estimate for variable-range hopping in the band tails. It can however be stated that the temperature dependence of the mobility does not exhibit a simple activation energy but a slope which decreases with

falling temperature, such that the tangent is proportional to (n+1) times the true hopping energy.

Finally, the conductivity associated with hopping in the band tails may be approximated as $ne\mu_{hop}$ where n is the total concentration of of electrons (cm^{-3}) in the band tails. The conductivity will contain the term $\exp(-(Em-E_f)/kT$. This activated temperature dependence will normally dominate over that from the mobility.

1.3.3 Conduction in Localized States at the Fermi Level

If there exists a finite density of defect-related states at the Fermi energy, transport can take place via (phonon assisted) hopping near this energy. As with hopping in the conduction band tail, the probability of an electron transition from one localized state to another at E_f is given by

$$\nu = \nu_{pH} \exp\left(-2\alpha R - W_{2/kT}\right) \tag{1.30}$$

where ν_{pH}, α and W_2 are defined as before. The mobility may be obtained from the Einstein relation as

$$\mu = \frac{eD}{kT} \quad \text{where} \quad D = \frac{1}{6}\nu R^2 \tag{1.31}$$

The conductivity may be obtained from $ne\mu$ and results in

$$\begin{aligned} \sigma &= \frac{1}{6} eR^2 \nu N(E_f) \\ &= \frac{1}{6} e^2 R^2 \nu_{pH} N(E_f) \exp\left(-2\alpha R - W_{2/kT}\right) \end{aligned} \tag{1.32}$$

At temperatures such that kT is less than half the width of the defect 'band', or if $N(E_f)$ is pinned between overlapping localized states, Eqn.1.32 leads to variable-range hopping, at least at sufficiently low T. As the temperature is lowered the number of phonons and their average energy will decrease. Carriers will tend to hop to larger distances in order to find states that are more energetically favourable. These states or sites are not likely to be nearest-neighbors. Nearest-neighbor hopping is only expected if $\alpha R >> 1$, which is not necessarily the case. The hopping energy W_2 is on the order of the bandwith and is written as

$$W_2 \cong \frac{1}{a^3 N(E_f)} \tag{1.33}$$

From Eqn.1.25 it is easily seen that the hopping range R increases with decreasing temperature. The derivation of the temperature dependence of the conductivity is as follows:

At temperature T the electron can hop to $4\pi R^3/3a^3$ sites, and the hop will be to a site which tends to minimize W_2. For this site

$$W_2 \simeq \frac{3}{4\pi R^3 N(E_f)} \tag{1.34}$$

with an average hopping distance $\bar{R}=3R/4$, so the actual probability of a hop per unit time is

$$\nu = \nu_{pH} \exp \left\{ -2\alpha R - W_2/_{kT} \right\} \tag{1.35}$$

Optimizing this expression yields

$$\bar{R} = \frac{3}{4}\left(\frac{3}{2\pi\alpha N(E_f)}\right)^{\frac{1}{4}} \tag{1.36}$$

Therefore the jump probability becomes

$$\nu = \nu_{pH} \exp\left(-\frac{B}{T^{\frac{1}{4}}}\right) \tag{1.37}$$

where

$$B = B_0 \left\{\frac{\alpha}{kN(E_f)}\right\}^{\frac{1}{4}} \quad \text{with } B_0 \simeq 2\left(\frac{3}{2\pi}\right)^{\frac{1}{4}} \tag{1.38}$$

The hopping conductivity can be obtained by multiplying Eqn.1.38 by $e^2 N(E_f)R^2$, such that

$$\sigma = \frac{1}{6} e^2 \bar{R}^2 \exp\left(-\frac{B}{T^{\frac{1}{4}}}\right) N(E_f) \tag{1.39}$$

It should be noted that the number of electrons per unit volume within kT of E_f was taken as $2N(E_f)kT$. B is expected to be constant over a restricted temperature range so that $N(E_f)$ may be considered constant over an energy range of approximatly kT. In this range ln σ versus $1/T^{1/4}$ is expected to be linear and to thereby indicate variable-range hopping at the Fermi level.

1.3.4 Conductivity Summary

The total conductivity is due to the summation of the individual modes of conduction. Plots of $\ln\sigma$ versus 1/T will illustrate the temperature dependence of the conductivity, with the appropriate activation energies in various regions of T as shown in Fig. 1.2 .

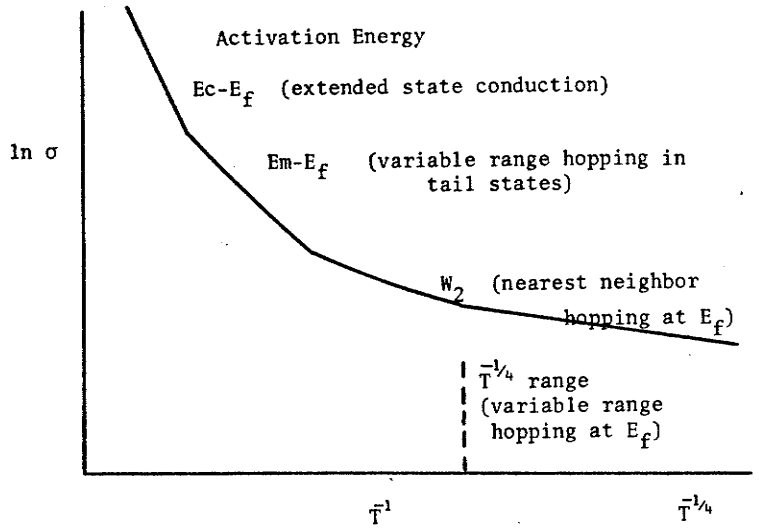

Figure 1.2: Illustration of ln vs. 1/T showing various activation energies.

1.4 DRIFT MOBILITY AND PHOTOCONDUCTIVITY

1.4.1 Drift Mobility and the Effect of Traps

When analyzing drift mobility, amorphous semiconductors are considered to have two types of traps. these are "intrinsic" traps (band tails) extending from Ec to E_A and deep traps due to defect states. At room temperature and above, hopping at the intrinsic traps may contribute appreciably, while deep trap hopping is considered to be negligible by comparison. The intrinsic drift mobility, due to extended-state and band-tail conduction, is written as

$$\mu_D \simeq \mu_{ext} \left(\frac{\Delta E}{kT}\right)^n \exp\left(-\frac{\Delta E}{kT}\right) + \mu_{hop} \exp\left(-\frac{W}{kT}\right) \qquad (1.40)$$

where $\mu_{ext} = \sigma_{min}/N(Ec)\cdot e$ at the mobility edge, $\Delta E = Ec - E_A$ and n arises from assuming a density of localized states of the form $N(E) \simeq (E-E_A)^n$. The hopping energy W is in general also a function of temperature.

Spear and Le Comber [22] observed a change in the slope (activation energy) of $\ln\mu_D$ versus 1/T at a particular temperature T_o on samples of r.f. glow-discharge-produced a:Si, deposited at a substrate temperature of 500 K. The dark conductivity also demonstrated a change at the same temperature T_o when plotted as $\ln\sigma$ versus 1/T. The interpretation was that above a critical temperature T_O the carrier transport was via extended states. The activation energy associated with the drift mobility was thought to be due to trapping in the shallow localized states, and hopping in the same states for $T<T_O$. These results were almost independent of deposition temperature T_d, and therefore arise not from defects, but rather from short-range order effects, since defect states (deep traps) are critically dependent upon T_d. Spear's work demonstrated agreement with Eqn.1.4.

1.4.2 Photconductivity

I_{PH} is defined as the excess current produced by radiation. One of the earliest reviews of photoconductive processes was written by A. Rose in (1951) [29], which dealt with photoconductivity in the presence of traps. In principle photoconductivity can yield information concerning trapping and recombination centers but often the interpretation is ambiguous. Interpretation is complicated by the variety of conditions under which measurements are made. Several important factors to consider are light intensity, wavelength,

sample geometry, contacts, magnitude of electric field, temperature and whether the experiment involves steady state or transient measurements.

In a simplified description two situations are of interest. Firstly when electrons and holes are trapped and do not escape, but rather recombine from these traps, (these traps are considered to be near the Fermi level), the photo current is then proportional to the rate of free electron hole pairs produced per unit volume F_o, (monomolecular recombination). In the second case, if the recombination rate of electrons is limited by the fraction of traps occupied by the holes (most being unoccupied) , the photocurrent is then proportional to $F_o^{1/2}$ (bimolecular recombination), for an intermediate range of light intensities.

1.4.2.1 Spectral Dependence of the Photoconductivity

Loveland et al. [22] reported in 1973 on the photoconductivity of r.f. glow-discharge produced a:Si(H). Their findings suggested an energy dependent quantum efficiency (η), as opposed to earlier reports.

The structure of the optical absorption coefficent α was evident in the photoconductivity curves, as well as the equation for the photocurrent [22]

$$I_{PH} = eF_o(1 - R)\left\{1-\exp(-\alpha d)\right\}\eta\tau/t_d \qquad (1.41)$$

Where F_o is the flux of incident photons ($cm^{-2}\,s^{-1}$), R is the reflectivity, τ is the recombination lifetime and t_d is the carrier transit time. Loveland's I_{PH} versus $\hbar\omega$ curves exhibited a shoulder between 1.1 and 1.3 eV with a rapid rise in I_{PH} at about 1.5 eV (corresponding to a rise in α). There was little or no evidence of an energy shift between a "photoconductivity edge" and the optical absorption edge. This may not be the case for films studied in the present thesis. Other than the shoulder in Loveland's photoconductivity curves no other structure was observed. Fischer and Donovan [30] (1972) also noted a shoulder in the photoconductivity curve of a:Si. Wronski et al. [31] (1977) reported on the optical and photoconductive properties of glow discharge produced a:Si thin films. Using Eqn. 1.41 they calculated $n\mu_n\tau$ which showed apparent structure at approximately 1.5 eV; this structure was dependent upon deposition temperature.

1.4.2.2 Temperature Dependence of the Photoconductivity

The majority of the discussion in this section derives from the work of Spear et al. [22,23] (1974) which is mainly concerned with glow discharge produced a:Si(H). A more general description is given by Simmons and Taylor [32] (1972), [33] (1974).

In Fig. 1.3 the photocurrent is shown as a function of 1/T. The excitation was confined to photon energies in the region of maximum photo-response ($\hbar\omega \simeq 2eV$).

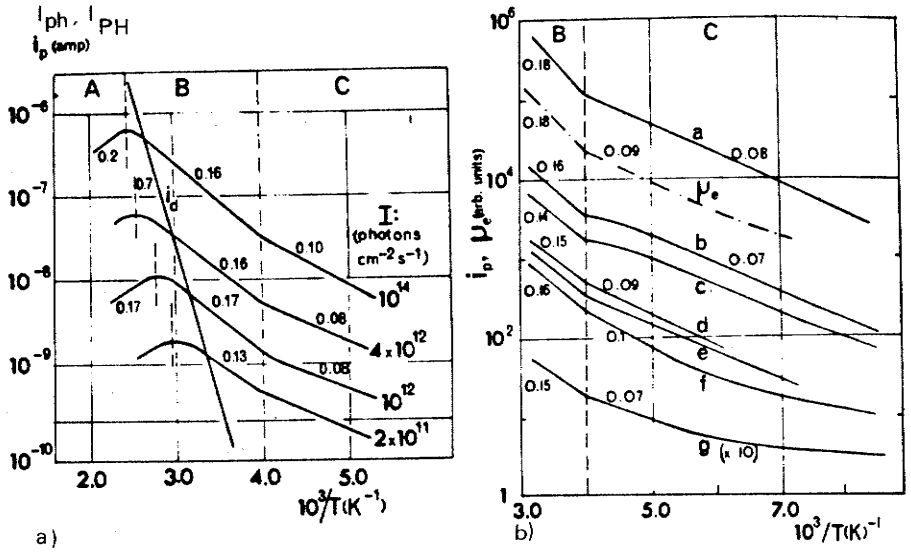

Figure 1.3: Photocurrent in a:Si plotted against the inverse temperature. Spear et al. [20-24]

Region A denotes the high temperature region, T>Tmax, where Tmax is the temperature corresponding to the photoconductivity maximum. Region B extends from Tmax down to about 250K. At 250K a well defined change in gradient is observed. Temperature range C is the region with T<250K.

The activation energy in region A was estimated [22] to be between 0.17 and 0.20 eV. In region B activation energies are between 0.18 and 0.14 eV. In region C the activation energy was found to be approximately 0.08 eV. In Fig. 1.3 b) a typical drift mobility curve has been included and shows a close similarity to the temperature dependence of I_{PH}. These curves were seen to be almost independent of photon energy of excitation ($\hbar\omega$). A gradual decrease in the activation energy was found at low temperature in region C.

In the analysis of photoconductivity recombination kinetics, consistent explanation of experimental results is pos-

sible only if transitions between localized (defect) states are included as well as transitions between extended and localized tail states. The following density of states model was used by Spear et al. to derive expressions for the recombination kinetics of glow discharge produced a:Si(H), as shown in Fig. 1.4 .

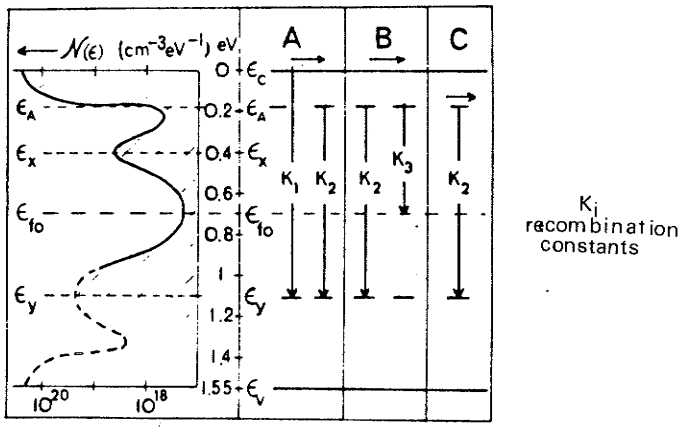

Figure 1.4:Schematic energy level diagram including the main features of the density of states distribution derived by Spear et al. [23] for r.f. glow discharge produced a:Si(H).

Temperature Range A

In the high temperature region T>Tmax, $I_{PH} << I_d$, the dark current, so that the state occupancies are almost those of thermal equilibrium (dark) conditions. This implies the quasi-Fermi levels for electrons and holes approximatly coincide with the thermal equilibrium Fermi level E_f . The transport in this region was found to be predominantly electron conduction in extended states at Ec. Therefore the

photoconductivity may be obtained by $\sigma_p = n_c e\mu_c$, where μ_c is approximately 5-10 $cm^2/V\text{-}s$. An electron at Ec recombining with a trapped hole at Ey, (localized defect state), yields a photoconductivity of the form

$$\sigma_p = \frac{eF_o\mu_c}{N_y K_1} \exp[(E_f - Ey)/kT] \qquad (1.42)$$

which implies an activation energy around 0.45 eV, whereas the experimentally determined value was found to be 0.2 eV [22]. If the electron was at E_A (bottom of localized tail states) and recombined with a hole at Ey, the photoconductivity would be of the form

$$\sigma_p = \frac{eF_o Nc}{K_2 N_y N_A} \mu_c \exp\left[\frac{-(E_f - E_y) - (Ec - E_A)}{kT}\right] \qquad (1.43)$$

which predicts an activation energy around 0.2 eV. Equation 1.43 also predicts a linear σ_p versus F_o relation. The linear relation between σ_p and F_o was experimentally observed in region A by Spear et al. [22,23].

Temperature Range B

In this range Spear et al. found that the photoconductivity and mobility yielded an activation energy of approximately $Ec-E_A$. They also noted a change from monomolecular to bimolecular recombination behavior as the illumination level increased. At high intensities the photogenerated carrier densities at Ec and Ev are larger than those in the dark, as a consequence of which the quasi Fermi levels will

separate from their dark value. States enclosed in energy by the two Fermi levels will have adjusted populations; states at E_A and Ey will become more populated at higher light intensities, making recombination between these two levels more likely. The photoconductivity becomes

$$\sigma_p = e\left(\frac{F_o}{K_2}\right)^{\frac{1}{2}} \mu_c \frac{Nc}{N_A} \exp\left[-\frac{(E_c - E_A)}{kT}\right] \qquad (1.44)$$

which predicts the correct activation energy and an approximately correct intensity dependence (high light intensity).

As previously mentioned the photocurrent tends towards a linear dependence on intensity at lower illumination levels. This effect can be explained by assuming that quasi-equilibrium is still a reasonable assumption. The lower temperature in region B compared with region A has caused a decrease in population at E_A and Ey but has left the population around E_f basically unchanged. Recombination through states at the Fermi level may now become important. If the density of states at E_f is $N(E_f)kT$ the photoconductivity may be dominated by the term

$$\sigma_p = \frac{eF_o Nc}{K_3 N_f N_A} \mu_c \exp\left[-\frac{(Ec - E_A)}{kT}\right] \qquad (1.45)$$

which gives a linear photocurrent-intensity dependence with the same activation energy as Eqn. 1.44.

Temperature Range C

A change in the gradient was observed by Spear et al. in the $\ln I_{PH}$ versus 1/T curve at around 250K. This same feature was also noted in the mobility. The gradient change was interpreted as a change in the predominant transport mechanism. The change in transport mechanism is from extended state conduction at Ec to electron hopping near E_A, as the temperature decreases. With decreasing T proportionately more carriers are located at E_A than Ec, and the thermal energy available (phonon population) to excite an electron from E_A to Ec decreases. This implies that at a critical temperature it will become more probable for an electron to hop to neighbouring localized sites than to be excited to an extended state at Ec.

The hopping mobility is given by

$$\mu_H = (\mu_H)_o \exp\left(-\frac{W}{kT}\right) \qquad (1.46)$$

where W is the hopping energy ($\simeq$0.09eV). The photoconductivity assumes the form $\sigma_p = n_A e \mu_H$, hence it may be written

$$\sigma_p = e \frac{F_o}{K_2}^{\frac{1}{2}} (\mu_H)_o \exp\left(-\frac{W}{kT}\right) \qquad (1.47)$$

Therefore the photoconductivity below 250K is controlled by the hopping activation energy W.

Current research in amorphous semiconductor photoconductivity has become too extensive to report comprehensively but the following are some examples of recent research in hydrogenated amorphous silicon: Photoconductivity in hydrogenated amorphous silicon-germanium alloys-Dong et al. [14] (1981), including a systematic study of related electrical properties; Optically-induced conductivity changes in hydrogenated a:Si -Wronski et al. [34] (1980); Studies of the temperature dependence of the photoconductivity of a:Si alloys -Griffith et al. [35] (1981); a:Si and a:Si_{1-x} Ge_x(H) photoconductivity studies by Moustakas, Paul et al. [36].

1.4.3 Photoconductivity and Recombination

The studies of Spear et al. [20-24] on hydrogenated amorphous Si have shown the possible existence of a recombination path between initial states at E_A to final states at Ey. The energy difference between these two states amounts to ten or more phonon energies in silicon; this implies a multiphonon recombination process, in the absence of radiative recombination. Mott has considered the problem of recombination in amorphous materials [36] (1975) and has found multiphonon recombination possible in principle. Mott also postulated that the presence of hydrogen may give rise to more energetic phonon modes as well as enhancing multiphonon processes.

1.5 OPTICAL ABSORPTION

The optical properties of an amorphous semiconductor are valuable tools in determining the electronic density of states. Parameters of interest are the real and imaginary parts of the dielectric constant. These parameters are related to the real and imaginary part of the refractive index which in turn determine to the optical absorption coefficient. In particular the imaginary part of the dielectric constant is proportional to the joint density of states (between initial and final states of an optically-induced electronic transition) and to the square of the appropriate momentum matrix element.

Methods of determining optical parameters include: (1) Kramers-Kronig analysis of reflectance curves, where the usual major limitation is that extrapolation is required outside the measurable spectral range; (2) The simultaneous determination of n and k from transmittance-reflectance curves, taking account of multiple coherent reflection inside the film and substrate. The results from this method are generally good, although an independent method for determining the film thickness is required; (3) Spectrally-resolved ellipsometry [43,44] where again multiple reflections are required to be accounted for. This method is accurate but the results are strongly affected by surface quality.

1.5.1 The Imaginary Part of the Dielectric Constant

The dielectric constant of a material may be written as $\varepsilon(\omega)=\varepsilon'(\omega)-j\varepsilon''(\omega)$, where the imaginary part, $\varepsilon''(\omega)$, is one of the most actively studied parameters of amorphous semiconductors. ω refers to the photon energy $\hbar\omega$ in the exciting radiation. In a crystal, the behavior of $\varepsilon''(\omega)$ is controlled to a large extent by the requirement of momentum conservation in optical transitions and by the form of the electronic density of states. In the amorphous phase, the structure determines the behavior of the momentum matrix elements which in turn specifies the nature of the transitions between filled and empty states. According to Hindley [37] the imaginary part of the dielectric constant $\varepsilon''(\omega)$ for an amorphous system can be written

$$\varepsilon'' \propto (M^a(\omega))^2 \int_o^{\hbar\omega} dE\, N_i(E) N_f(\hbar\omega - E) \qquad (1.48)$$

whereas ε'' for a cyrstalline system is

$$\varepsilon'' \propto (M^c(\omega))^2 \int dk\, \delta[E_f(\bar{k}) - E_i(\bar{k}) - \hbar\omega] \qquad (1.49)$$

where $M^a(\omega)$ and $M^c(\omega)$ are the amorphous and crystalline momentum matrix elements, and $N_i(E)$ and $N_f(\hbar\omega-E)$ are the initial and final density of states separated by an energy $\hbar\omega$.

By comparing Eqn. 1.48 with Eqn. 1.49 it can be seen that energy is conserved in the transitions in both cases, but the k conservation requirement of the crystalline case is absent in the amorphous case. The joint density of states

in the crystalline case has been replaced by a convolution of the density of states in the valence and conduction bands for which energy is conserved.

An interesting result presented by Hindley is the continuity of the average momentum element when going from delocalized-to-delocalized transitions to localized-to-delocalized transitions. This implies no break will appear in $\varepsilon''(\omega)$ at the mobility gap.

The amorphous ε'' characteristic may be viewed as a modified crystalline ε'' characteristic. The major modification arises from relaxing the k conservation rule which is equivalent to smoothing out the momentum matrix elements for the crystal case, but retaining approximatly the same energy dependence.

In theory the density of states may be calculated from the ε'' curve using Eqn. 1.48. In order to evaluate Eqn. 1.48, $M^a(\omega)$ is required. $M^a(\omega)$ is an average matrix element depending on the momentum operator between two localized functions at the same site. It is argued that $M^a(\omega)$ can be represented by a smoothed version of the crystalline matrix element $M^c(\omega)$, where the smoothing is due to lack of long range order. An example of this procedure is given by Connell et al. [38] (1974). A typical result for ε'' for the amorphous and crystalline states is shown in Fig. 1.5 .

In general the ε'' curves for amorphous materials exhibit far less structure than their crystalline counterparts. The

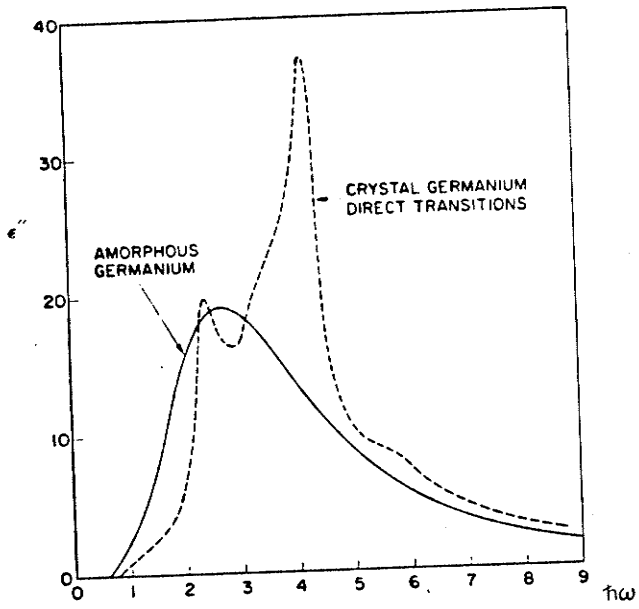

Figure 1.5: ε'' as determined by Kramers-Kronig analysis of reflectance data for amarphous Ge (solid line) and crystalline Ge (dashed line), Donovan and Spicer [39] (]970).

gross features are often preserved. As shown in Fig. 1.5 the basic shape of the ε'' curve is maintained although the crystalline peak due to direct (k conserving) transitions is absent altogether. This interesting feature can be used to obtain a qualitative understanding of the density of states or types of disorder. The first peak in ε'' for the crystalline case is caused by indirect transitions in the crystallographic direction (111) whereas the second peak is caused by direct transitions in the (100) directions. The absence of the second peak in the amorphous phase may indicate a greater disorder in the (100) direction of the unit cell. Indications of the relaxation of the k conservation rule can be found by comparing the ε'' curves for the crystalline and amorphous states: namely, the sharp features in the ε'' spectrum for the crystalline case, which can be correlated

with theory to infer the band structure (E vs. k) is absent in the amorphous phase. The observed behaviour of ε'' in the energy range of interband transitions provides evidence for relaxation of the k conservation selection rule.

1.5.2 The Absorption Coefficient

The most interesting features of optical absorption in amorphous semiconductors arise from the relaxation of the k conservation selection rule discussed above. In the case of some amorphous semiconductors (eg. those prepared by quenching from the melt) a gradual increase in the absorption coefficient below the (crystalline) optical gap is often observed (refered to as an Urbach edge or exponential edge). Reasons for this effect in crystals can be the Franz-Keldysh effect, electron-phonon coupling, exciton-line broadening or bound exciton interaction with lattice vibrations [1,40]. Many authors have suggested that the exponential edge in amorphous semiconductors is due to electronic transitions between localized states in the band tails. There is much controversy over the origin of the absorption edge, and it is unlikely that this situation will improve in the near future. For a further discussion on the exponential edge the reader is referred to Mott (1) and Connell (40).

Regarding amorphous Si or Ge, there exists a diversity in published optical absorption data that is perhaps unequalled in the literature on amorphous semiconductors. One reason

for the diversity is the difficulty in determining the optical parameters because sufficiently thick homogeneous films are not available. Thickness limitations imposed on films prepared by conventional deposition techniques (sputtering, plasma or vapor deposition) make it difficult to obtain accurate absorption data below $\alpha = 10^3\,cm^{-1}$. Additional variations in data arise from the differences in the method of preparation and of subsequent film treatment.

The following discussion is concerned with the optical absorption edge expected in materials which do not exhibit an exponential absorption tail, or materials which do exhibit an exponential tail but where the photon energy of interest is well above the exponential tail region. Assuming a relaxed k conservation rule and constant matrix elements for transitions between states in different bands, the absorption coefficient can be expressed (at least over a small energy range) according to Mott and Davis [1] as

$$\alpha(\omega) \propto \frac{8\pi^4 e^2 \hbar a}{n_o cm^2} \int_{c,v} dE \, \frac{Nv(E)Nc(E + \hbar\omega)}{\hbar\omega} \qquad (1.50)$$

Under the assumption of parabolic ($E \propto k^2$) bands Eqn. 1.50 reduces to [1]

$$\hbar\omega\alpha(\omega) \propto (\hbar\omega - E_{opt})^2 \qquad (1.51)$$

The absorption in many amorphous materials is observed to obey this relation above the exponential tails. The quantity E_{opt} has been defined as an optical gap, even though it may not represent a zero in the density of states.

Mott and Davis [1] have derived a similar quadratic dependence by assuming that the density of localized tail states are linear functions of energy with N(Ec)=N(Ev) and with the range of tail states expressed as ΔE. Their expression for the absorption coefficient is

$$\alpha(\omega) = \frac{4\pi}{n_o c} \frac{\sigma_{min}}{\hbar\omega\, E} (\hbar\omega - E_{opt}^{*})^2 \qquad (1.52)$$

where E_{opt}^{*} is the energy difference between the bottom of the localized tail states (E_A) and the valence band (Ev), and

$$\sigma_{min} = \frac{2\pi^3 e^2 \hbar^3 a}{m^2} \left\{ N(Ec) \right\} \qquad (1.53)$$

This quadratic behavior is not characteristic of all amorphous materials and as such can not be regarded as a universal phenomenon.

Without prior knowledge of the density of states or of the transition matrix elements, the exact meaning of an optical gap can not be defined. The $\alpha(\omega)$ relation is in any case of fundamental importance both to the actual density of states, and in its relation to the mobility gap discussed in the above sections.

For photon energies below E_{opt}, the absorption in almost all materials varies exponentially with energy as

$$\alpha(\omega) \propto \exp\left[-\beta(Ee - \hbar\omega)\right] \tag{1.54}$$

where Ee is approximatley E_{opt}. Typical values of β are 10-25 eV . This absorption is often related to the Urbach edge [17].

One explanation of the origin of the exponential absorption region is based on the effects of the disorder-induced potential fluctuations [17]. This may be modeled by effective donors and acceptors, where electron wave functions are exponentially attenuated in the regions where hole wave functions are large and vice versa. The low energy optical transitions between valence states near potential maxima and conduction states near potential minima at effective donor-acceptor pairs, then may be treated by dipole interactions.

The literature contains many qualitative descriptions of the optical absorption process. Complexities that arise in determining the density of states stem both from assumptions regarding matrix elements and experimental difficulties. Despite these problems optical measurements and their interpretation are invaluable tools in developing an understanding of amorphous semiconductors.

Chapter II

DISPERSION OF THE OPTICAL CONSTANTS OF a:S_{1-x} Ge_x (H)

2.1 EXPERIMENTAL TECHNIQUES

The hydrogenated a:$Si_{1-x}Ge_x$(H) alloy films were fabricated by Dr. H. Watanabe [1] on optically flat glass substrates by radio frequency (r.f.) sputtering in a gas mixture of argon and 5% hydrogen at a pressure of 6 x 10^{-3} torr. The Ge content (x) was varied by varying the total area of the Si segments placed on a Ge wafer target [41]. The substrate temperature was maintained between 220 °C and 240 °C and the film thickness ranged from 1.6 μm to 2.4 μm. The mole fraction of the Ge content (x) was estimated by

$$x \simeq \frac{\eta_{Ge} A_{Ge}}{\eta_{Ge} A_{Ge} + \eta_{Si} A_{Si}} \qquad (2.1)$$

where A_{Ge} and A_{Si} were the target areas of Ge and Si respectively, η_{Si} and η_{Ge} are the sputtering efficiencies of Si and Ge which are 0.53 atoms/ion and 1.22 atoms/ion for Ar ions with a kinetic energy of 600 eV, respectively. This equation provides only a rough estimate of x. The actual value of x quoted in this report was determined by measuring the X-ray flourescence intensity of the Ge-Kα line, which

---

[1] Sendai Radio Technical College, Kami-Ayashi Miyagi-Ken, Japan.

has been shown [42] to be linearly proportional to the weight of the Ge in the films. The amorphous structure was confirmed by X-ray analysis. The films were reported to contain oxygen as an unavoidable impurity; using secondary emission X-ray analysis the films were also seen to contain argon as an impurity.

The optical constants were measured using the same techniques reported by Kao and Adashi [43] which is described briefly as follows: A Gaertner model L119 ellipsometer and a model L135W Babinet-Soleil compensator were used in conjunction with a Bausch-Lomb grating monochromator. A xenon arc lamp was used as a source for the wavelengths $0.35 \leq \lambda \leq 1.0$ μm, while a mercury arc lamp and a mica quarter-wave plate were used for measurements at 5461 Å. The ellipsometer measurements were made by null setting the polarizer and analyzer which yielded two characteristic parameters: Δ defined as phase angle change and ψ defined as the arctangent of the amplitude ratio, of the reflection coefficients in the plane of incidence, and perpindicular to this plane [44]. The three unknown constants involved were the refractive index n, the extinction coefficient k and the film thickness d. In order to obtain n and k from Δ and ψ the film thickness d was established independently.

The film thickness was estimated by weighing the substrate before and after deposition and calculated from the known data of film surface area, the Ge content and the Si

and Ge densities. The film thickness was also estimated by examining interference fringes obtained from spectrophotometry measurements at wavelengths considerably greater than the optical transmission cutoff [43]. The film thickness was then calculated from [43]

$$\frac{1}{2nd} = \left(\frac{1}{\lambda_1} - \frac{1}{\lambda_2}\right)^{-1} \qquad (2.2)$$

where λ_1 and λ_2 are the wavelengths at successive interference maxima and n is the index of refraction approximated by the index of refraction for the crystalline case. Consistent estimates of the film thickness were obtained.

With the estimated value of d and measured null setting analyzer and polarizer angles, a Fortran program [44] was used to yield accurate values of n and k over preset limits. The angle of incidence was than changed and new values of n and k were determined.

The absorption coefficient of a:Si(H) at 1.0μm was approximately 2×10^4 cm^{-1} and rapidly increased to about $10^5 cm^{-1}$ for decreasing wavelength. This high value of absorption corresponds to a light intensity at the opposite surface of only 10^{-4} of the incident light intensity. The absorption coefficient for films with x>0 were much larger than that for the a:Si(H) film (with x=0) so that for most wavelengths the film thickness could be considered to be essentially infinite. Although the infinite thickness model would have yielded sufficiently accurate results, the model

used was nevertheless that of a finite thickness film on a glass substrate. The possibility of multiple reflections were also accounted for. A surface oxide layer was not included in the calculations. According to Connell et al. [65] the observed trends should be correct in this intepretation, although the absolute values and finer details of the variations of n and k cannot be accurately determined. The oxide layer did not present a problem in this study, since only gross variations and trends of n and k were required. Since the films were extremely absorbing, the effect of any error in the estimation of the film thickness was also minimized.

The shortest wavelength employed was 0.35 μm, which was limited by the optical elements of the ellipsometer, whereas the longest wavelength, 1.0 μm, was limited by the sensitivity of the Si photodetector. In most of the material investigated this wavelength range covered photon energies both appreciably larger and smaller than the optical band gap, and in all cases, the dispersion of n and k in this wavelength range proved to be of considerable interest. For wavelengths longer than 1.0 μm, data was obtained from the interference fringes observed in spectrophotometer measurements. All optical measurements were made in an otherwise dark room at room temperature.

2.2 EXPERIMENTAL RESULTS

The results for the optical constants can also be found in [45]. The complex refractive index is defined as follows

$$n^* = n - jk \tag{2.3}$$

where the real part is the refractive index and the imaginary part is the extinction coefficient. These optical parameters derived from the ellipsometric parameters Δ and ψ are shown as functions of photon energy in Figs. 2.1 and 2.2.

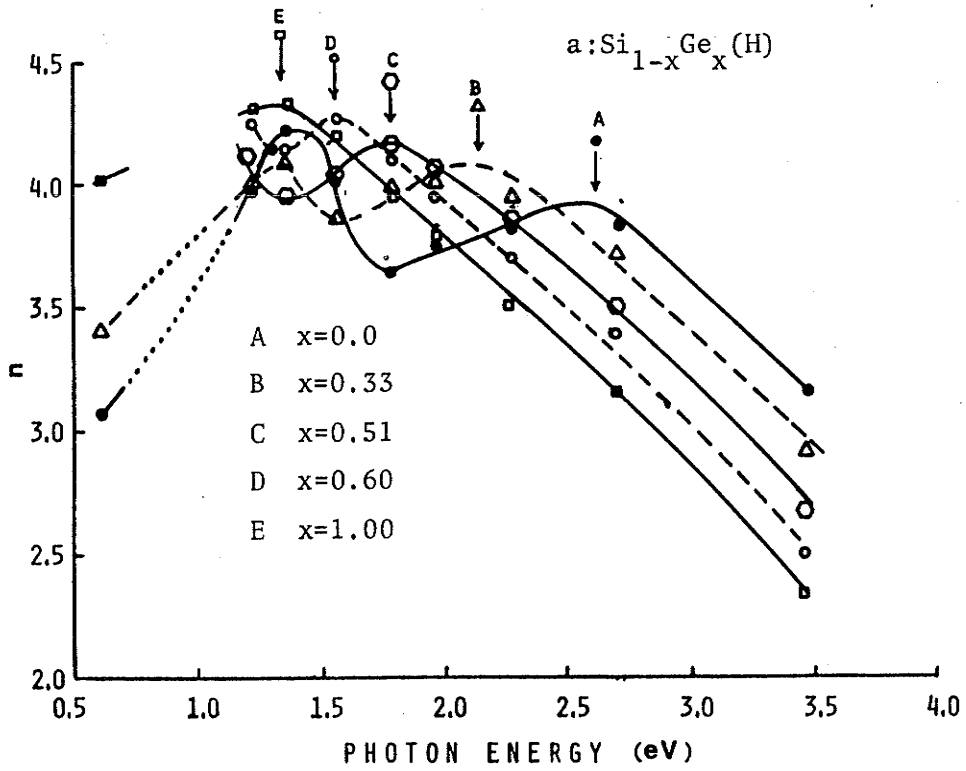

Figure 2.1:The real part of the refractive index (n) as a function of photon energy for a:$Si_{1-x}Ge_x$(H)

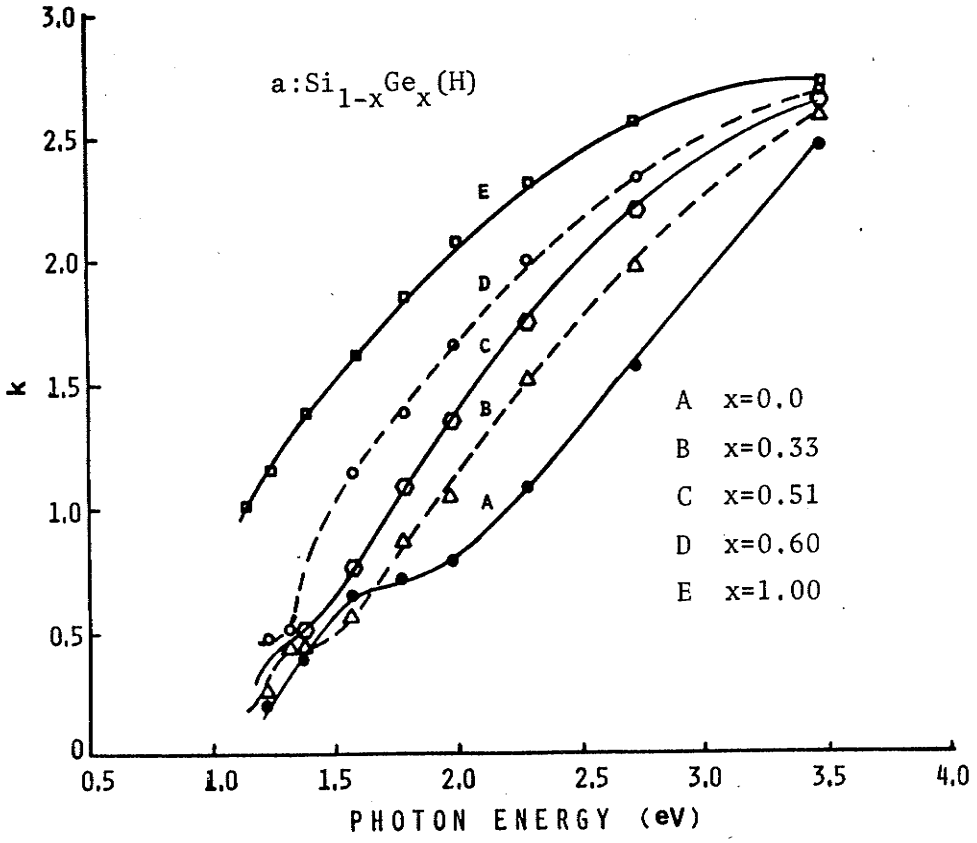

Figure 2.2:The extinction coefficient as a function of photon energy for a:$Si_{1-x}Ge_x$(H)

It can be seen that both n and k are dispersive; n exhibits two peaks in its spectra while k exhibits a high energy peak and structure at low photon energies. As the lowest photon energy that could be used for the ellipsometric measurements is 1.24 eV (λ=1.0μm) the data extending to 0.6 eV was deduced from the interference fringes in the spectrophotometric measurements.

In Fig. 2.1 it is clear that for a:Si(H) the first peak of n occurs at a photon energy of 2.6 eV and the second peak occurs at 1.4 eV; for a:$Si_{0.67}Ge_{0.33}$(H) the first peak occurs at 2.1 eV while the second peak is believed to occur at approximately 1.3 eV. In Fig. 2.2 , although the first peak

in the spectra of k could not be observed because the highest available photon energy was 3.5 eV (limited by the optical elements of the ellipsometer) the curves do imply the existence of a peak beyond 3.5 eV. This is consistent with the fact that a peak in k for a:Ge at a photon energy of 4 eV has been observed by Connell et al [65]. It is interesting to note that there is structure and in some cases a second peak at lower photon energies, which corresponds to the second peak in n.

Plots of the first and second peak values of n and their corresponding photon energies, n_p and E_p, as functions of composition x are shown in Fig. 2.3 . It can be seen that both n_p and E_p vary linearly with composition. Such a near-linear dependence upon composition is also observed for n and k at a fixed photon energy (2.6 eV) as shown in Fig. 2.4 . The data of curve B in Fig. 2.4 were deduced from the interference fringes in the spectrophotometric measurements at a photon energy of approximately 0.6 eV.

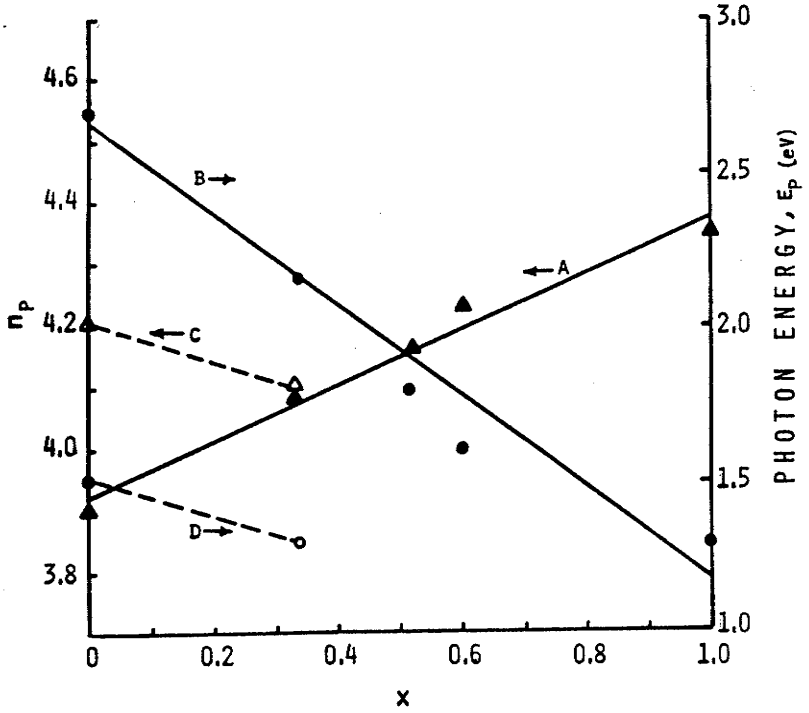

Figure 2.3:The peak value of the refractive index n_p and the corresponding photon energy E_p for its occurrence as functions of composition of a:$Si_{1-x}Ge_x(H)$ films. A, the first peak value of n; B, the photon energy for the occurrence of the first peak in n; C, the second peak in n; D, the photon energy of the second peak.

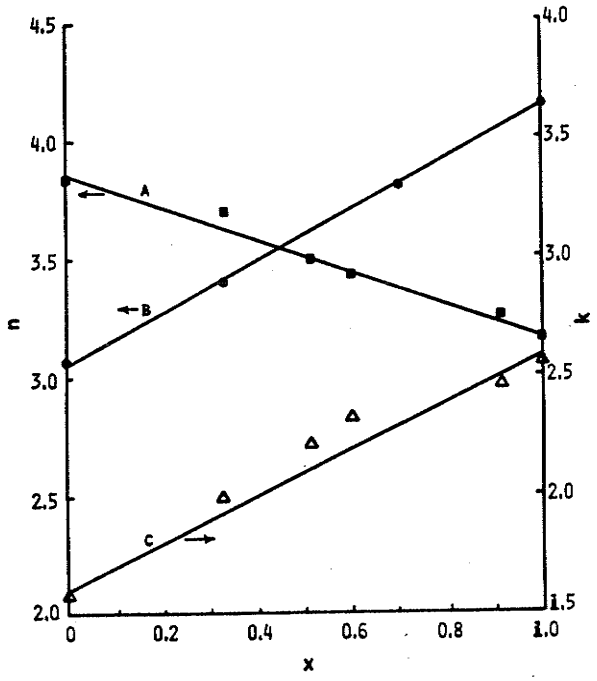

Figure 2.4:Refractive index and extinction coefficient as functions of composition. A, n @ 2.708eV; B, n @ 0.606eV; C, k @ 2.708eV.

The complex dielectric constant is defined by

$$\varepsilon^* = \varepsilon' - j\varepsilon'' \tag{2.4}$$

where the real part ε' is the dielectric constant and the imaginary part ε'' is the loss factor. By means of the relation $\varepsilon^* = n^{*2}$, ε' and ε'' are easily expressed in terms of n and k as follows

$$\varepsilon' = n^2 - k^2$$
$$\varepsilon'' = 2nk \tag{2.5}$$

From the data for n and k, ε' and ε'' have been calculated and are shown as functions of photon energy in Figs. 2.5 and 2.6 .

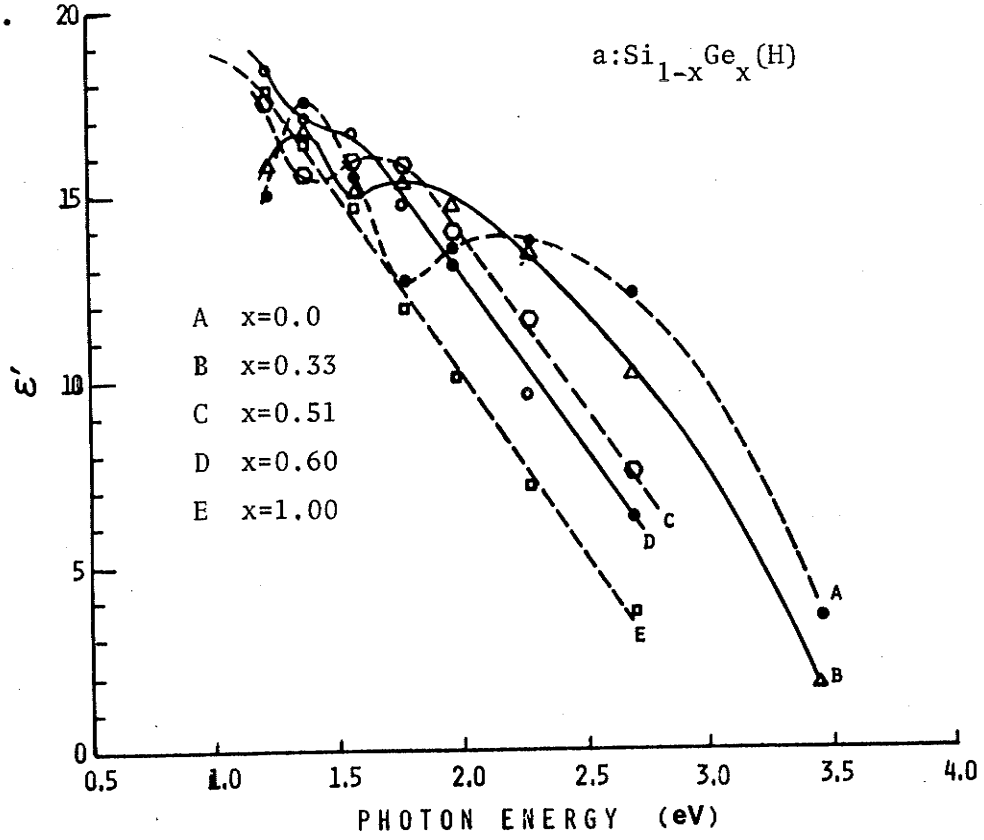

Figure 2.5:The real part of the dielectric constant

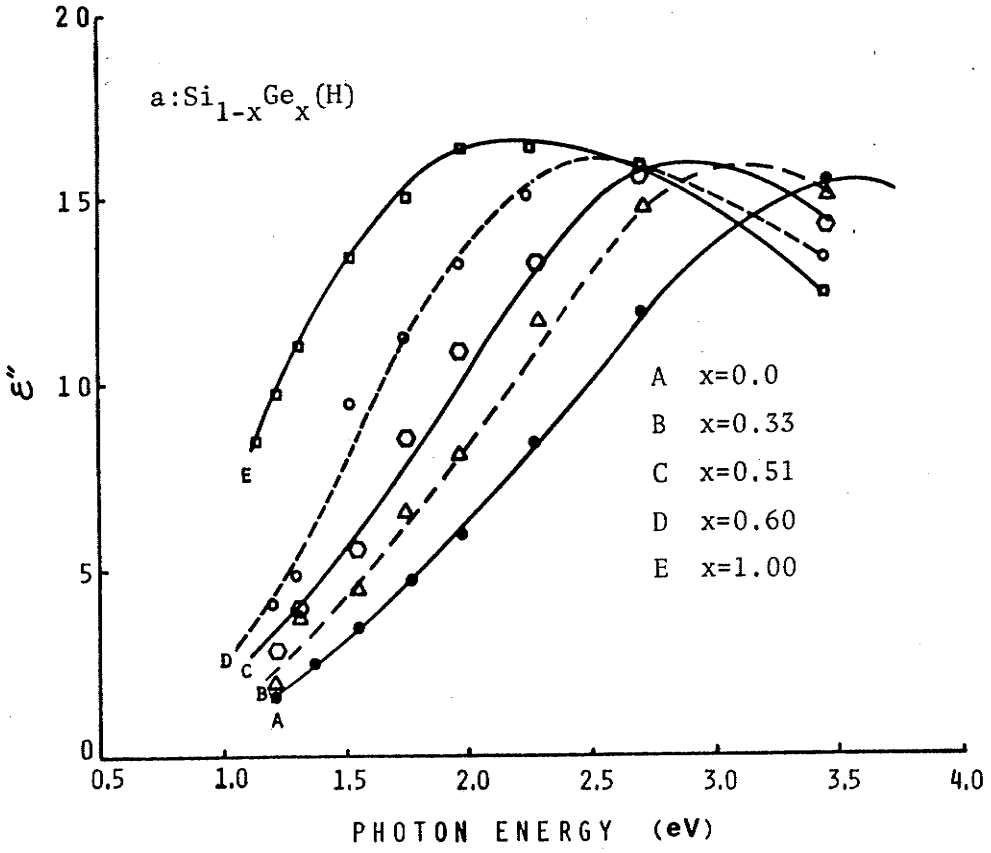

Figure 2.6 Imaginary part of the dielectric constant for a:$Si_{1-x}Ge_x$(H)

The absorption coefficient α can be related to the extinction coefficient k by [43]

$$\alpha = \frac{4\pi k}{\lambda} \qquad (2.6)$$

where λ is the free space wavelength of the exciting radiation. The absorption coefficient has been calculated for various photon energies using the experimental data for k; the results are shown in Fig. 2.7 .

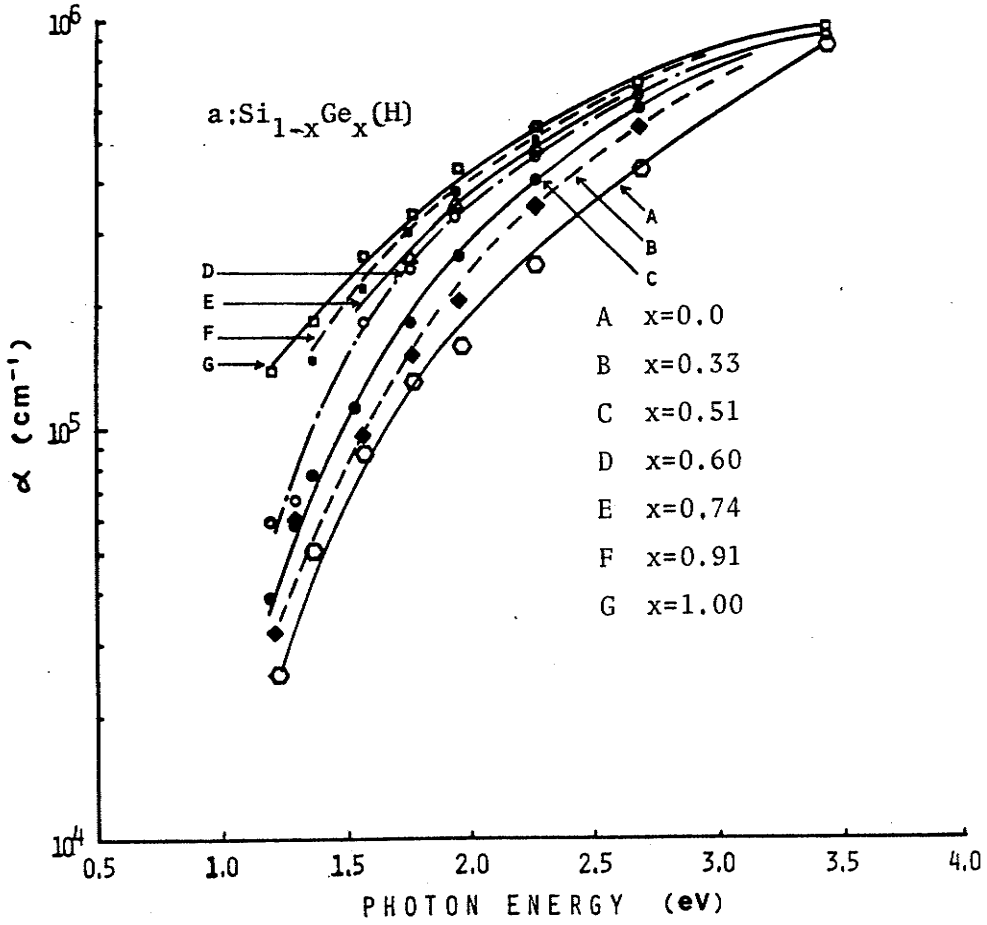

Figure 2.7:The absorption coefficient as a function of photon energy for a:$Si_{1-x}Ge_x(H)$

Figure 2.8 shows the value of α at a fixed photon energy of 1.96 eV, and the photon energy $\hbar\omega$ for a fixed value of α as functions of composition x. The fixed photon energy of 1.96 eV was selected in order to compare the results of the present study with the results of Beaglehole and Zavetova [15] which are also included in Fig. 2.8 . It can be seen that there is an approximately linear dependence on x and reasonably good correlation between the two sets of results.

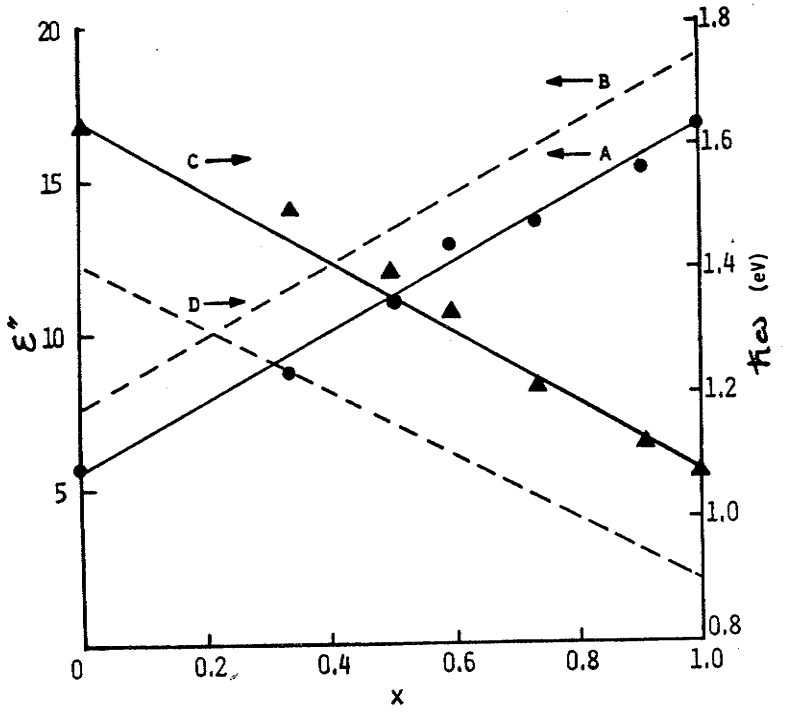

Figure 2.8: Loss factor ε'' at a photon energy of 1.96eV, and the photon energy $\hbar\omega$ at a fixed value of α as functions of composition for a:$Si_{1-x}Ge_x$(H) films. A, ε''-present study; B, ε''-Beaglehole and Zavetova [15]; C, $\hbar\omega$ present study $\alpha=10^5 cm^{-1}$; D, $\hbar\omega$ from [15] for $\alpha=10^4 cm^{-1}$.

Assuming parabolic bands for the extended states, the absorption coefficient conforms to the relation [1]

$$\alpha(\omega)\hbar\omega = A\,(\hbar\omega - E_{opt})^2 \qquad (2.7)$$

where $\hbar\omega$ is the photon energy, E_{opt} is the so-called optical gap, and A is a constant for a given film composition x. Tabulated values of A are given in Fig. 2.9 , and are observed to decrease monotonically as the Ge content is increased. An estimate of the extent of the localized tail states ΔE is obtained by assuming that their densities at the band edges are linear functions of energy which leads to [1]

$$\Delta E = \frac{4\pi}{nc} \frac{1}{A} \sigma_{min} \qquad (2.8)$$

By assuming a value of 200 $\Omega^{-1}cm^{-1}$ for σ_{min} and expressing energies in electron volts, values for ΔE were calculated and are given in Fig. 2.9 . The values of ΔE are observed to generally increase with increasing x. Although the variation of ΔE with respect to x is not great the variation of ΔE with respect to the total band gap (which decreases with x) is significant. A plot of $(\alpha \hbar\omega)^{1/2}$ versus $\hbar\omega$ is given in Fig. 2.9 for $Si_{1-x}Ge_x(H)$ films for various values of x. The dependence of $(\alpha\hbar\omega)^{1/2}$ upon $\hbar\omega$ is linear only for a certain range of photon energies which is dependent upon composition x. For x=0, this dependence becomes nonlinear for $(\alpha \hbar\omega)^{1/2} < 1000\ eV^{1/2}\,cm^{-1/2}$, and for x=0.51, it becomes nonlinear for $(\alpha \hbar\omega)^{1/2} < 500 eV^{1/2}\,cm^{-1/2}$. By extrapolating the linear portion of the curves in Fig. 2.9 to $(\alpha\hbar\omega)^{1/2}=0$, the optical band gap E_{opt} was obtained for each curve as the intercept with the abscissa. The values of E_{opt} as a function of x are shown in Fig. 2.10 . Results for the optical band gap for $a:Si_{1-x}Ge_x(H)$ films fabricated by r.f. glow discharge reported by Chevallier et al.[16] are also included in Fig. 2.10 for comparison.

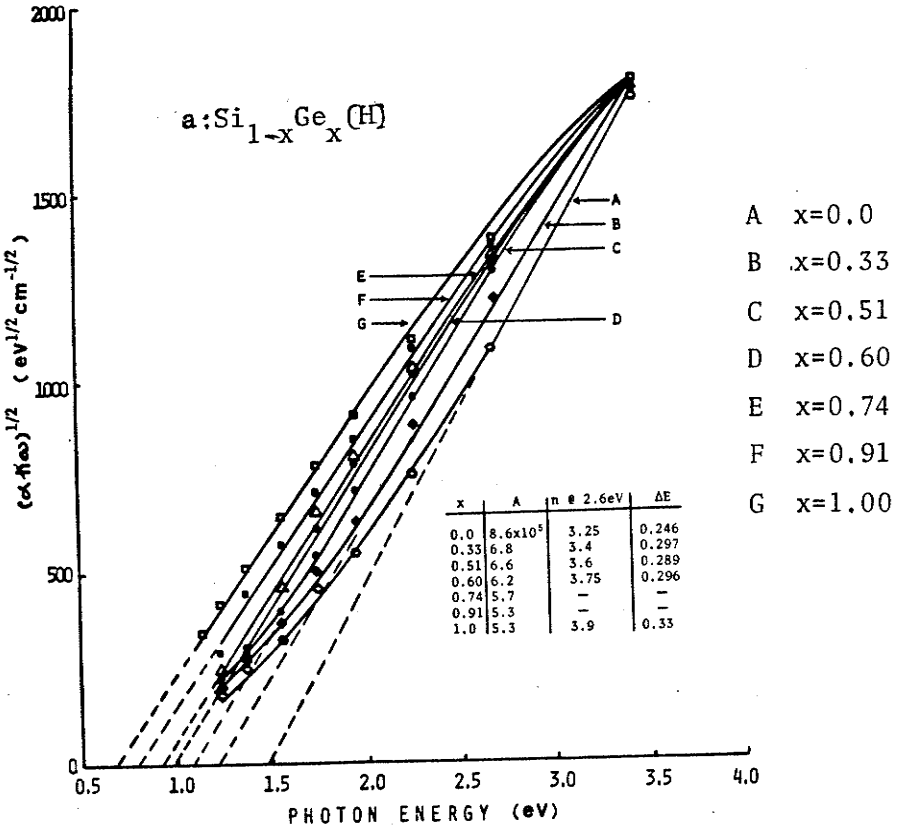

Figure 2.9: $(\alpha\hbar\omega)^{1/2}$ as a function of photon energy for a:$Si_{1-x}Ge_x$(H)

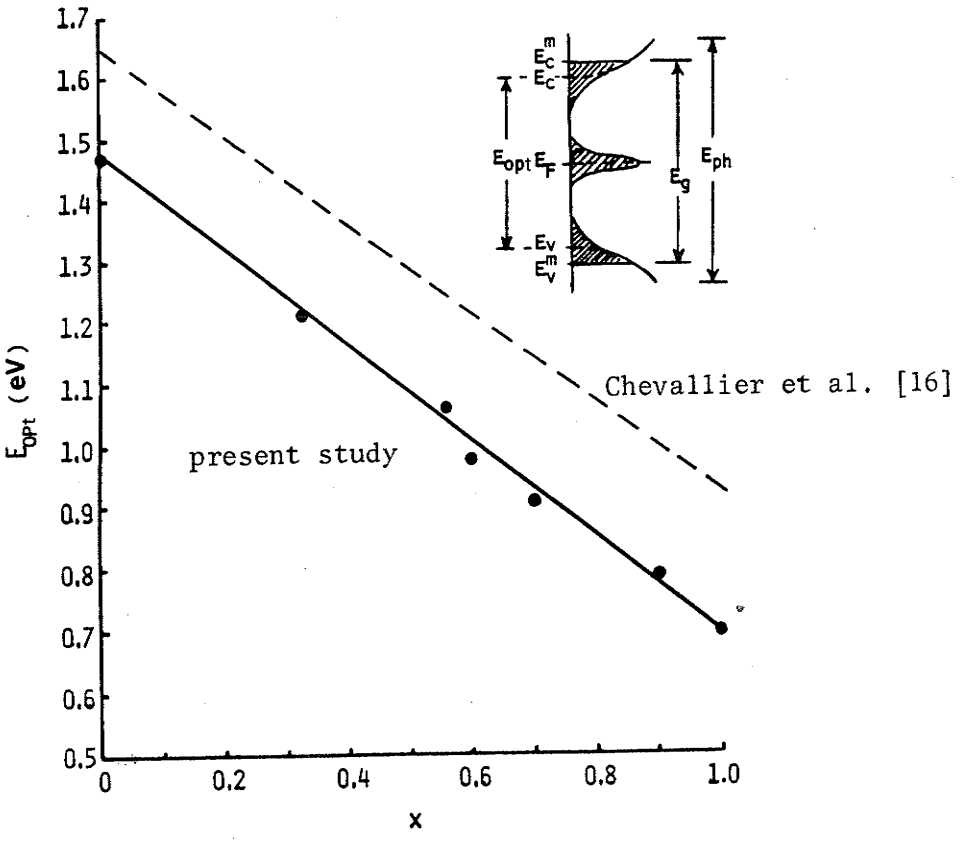

Figure 2.10 E_{opt} as a function of composition

2.3 DISCUSSION

It is convenient at this point to review some theoretical and experimental observations which are generally accepted, concerning the optical properties of non-crystalline materials:

1) Most materials including Si, Ge and their alloys exhibit lower dark- and photo-conductivities in their amorphous phase than in their crystalline phase, indicating that disorder creates localization within the forbidden region between the band edges. This is often expressed as the existence of localized gap states due to disorder or defects.

2) Sharp absorption edges which arise from interband transitions between states localized in k-space for materials in the crystalline phase disappear in their amorphous phase. This is expressed as the existence of localized tail states due to a lack of long range order, or as a relaxation of the selection rule for conservation of crystal momentum k.

3) At photon energies in excess of the absorption edge, the optical absorption data for many amorphous materials follow Eqn. 2.6, indicating that the band structure in the neighborhood to the mobility edges is parabolic.

Evidence for the relaxation of the k conservation rule can be derived by comparing the absorption coefficient in the amorphous and crystalline phases. The absorption edges in crystalline Ge are at 0.66 eV across an indirect gap and

0.80 eV across a direct ($\Delta k=0$) gap, and those of Si are at 1.1 eV and 3.0 eV corresponding to indirect and direct gap transitions, respectively [47]. These materials, as well as Si-Ge alloys in the crystalline phase, obey the selection rules based upon k conservation [48] and therefore exhibit two peaks in the spectra of ε'' corresponding to the transitions in the [111] and [100] directions [1,2]. However, these materials in the amorphous phase exhibit only one peak in the spectra of ε'' and show far less structure indicating that the disorder is sufficient to smear out fine structure and to produce broadening in k-space [35,36,39], thus resulting in a smooth absorption band as shown in Fig. 2.6

Optical absorption results primarily from interband transitions or from transitions to and from localized states within the mobility gap. Such transitions at certain photon energies produce exciton-like bound electron-hole pairs, which may either dissociate into free carriers or recombine to annihilate each other, under the influence of thermal agitation and applied electric fields. Another possibility is that transitions to or from localized states within the mobility gap may create exciton-like free carrier-trapped carrier pairs. It is these exciton-like pairs which act as dipoles and thus result in the dispersion in n and k. The dissociation efficiency of such photo-generated electron-hole pairs bound by their Coulombic attraction depends on the initial thermalization distance (or orbital radius) r_o

between the charged carriers. Similarly the dissociation efficiency of carrier-trap pairs depends on their initial thermalization distance. It is reasonable to assume that r_o increases with increasing photon energy. Obviously the larger the value of r_o the higher is the probability for the photogenerated electron-hole pairs to dissociate into free carriers, and hence higher the is the quantum efficiency for photoconduction. By assuming that energy is conserved during the optical transition and that the optical transition matrix elements are constant over the energy range of interest the relation of ε''or α to the photon energy and density of states can be written as

$$\begin{aligned} \alpha(\omega)n &= \frac{\omega^2\varepsilon''}{c} \\ &= B_1 \int Nc(E)Nv(\hbar\omega - E)dE \\ &+ B_2 \int N_g(E)Nc(\hbar\omega - E)dE \\ &+ B_3 \int Ng(E)Nv(\hbar\omega - E)dE \end{aligned} \tag{2.9}$$

where Nv(E), Ng(E), Nc(E) are the densities of states in the valence band, the mobility gap and the conduction band respectively; B_1, B_2, and B_3 are constants which are independent of E, but may depend on photon energy $\hbar\omega$. The first term on the right-hand side of Eqn. 2.9 can be interpreted as the probability for the optical transitions at the exciting photon energy $\hbar\omega$ between holes in the valence band and electrons in the conduction band, the second term as the

probability for transitions from the valence band to gap states, and the third term as the probability for transitions from the gap states to the conduction band. Figures 2.7 and 2.9 show that the rate of increase of α and $(\alpha\hbar\omega)^{1/2}$ with respect to increasing photon energy tends to diminish at photon energies higher than about 2 eV. Although these parameters were not measured for photon energies greater than 3.5 eV due to measurement system limitations it can be clearly seen that ε'' deduced from the measured parameters n and k exhibits a peak in its spectrums for all x as shown in Fig. 2.6 . The photon energy at which the peak of ε'' occurs may be interpreted as the location at which the rate of change of the effective states available for optical transitions is a maximum. This photon energy is denoted E_{PH}, to distinguish it from E_{opt} , which is the energy separation between Ec and Ev. Both E_{PH} and E_{opt} are shown schematically in the insert of Fig. 2.10 . The energy range around the peak of ε'' can be considered to be the energy range for interband transitions, and it is assumed that only the first term of the right-hand side of Eqn. 2.10 is dominant in this energy range. For photon energies higher than E_{PH}, ε'' decreases with increasing $\hbar\omega$ since for $\hbar\omega > E_{PH}$, α increases more slowly with increasing $\hbar\omega$ indicating that Nc(E) and/or Nv(E) have attained their maximum values and tend to decrease with increasing E. For photon energies lower than E_{PH}, ε'' and α are seen to increase with increasing photon

energy because the density of effective states available for optical transitions is also increasing.

The parameters k and α are directly related to the photogeneration of electron-hole pairs or carrier-trap pairs, regardless of whether or not these pairs dissociate and recombine or form excitons with subsequent geminate recombination. On the other hand ε'' is not only related to absorption but is also effected by the exciton-like behavior of the photogenerated bound electron-hole pairs or carrier-trap pairs. The effect of these bound pairs on ε'' is believed to be second-order, with absorbtion being a first-order effect; the effect of these bound pairs is believed to be much more pronounced on ε'. For exciting photon energies above the optical band gap, the recombination of free electrons and free holes is not bimolecular, but is most likely monomolecular via localized states in the mobility gap. These transitions are mainly non-radiative so that the major portion of the energy released from the recombination is lost in the form of heat. However, the recombination of bound electron-hole pairs is equivalent to the collapse of excitons and the transitions could be primarily radiative. It is assumed that the major portion of this type of recombination is converted to radiation energy which may be reabsorbed by the material to form new electron-hole pairs, thus the net loss of energy is small and hence the steady state absorption of exciting photons is also small. For photon

energies less than E_{opt}, the absorption is mainly between localized states in the mobility gap and extended states in either the valence or conduction band. The bound carrier-trap pairs produced by such transitions are much more strongly bound by their mutual Coulombic attraction than those produced by interband transitions, since in the former case only one type of carrier is mobile, while the other carrier is trapped. The behavior of these carrier-trap pairs is much like that of excitons. It is reasonable to assume that the major portion of energy released after annihilation of such bound carrier-trap pairs will be radiative and reabsorbed by the material in order to form new bound carrier-trap pairs. Therefore, it is expected that the net steady-state absorption would be small in the energy range of photon-induced transitions between localized states in the gap and extended states. This expected result based upon radiative recombination is consistent with the small second peak in k as shown in Fig. 2.2 , at least for small values of x. Further evidence of exciton-like behavior of electron-hole pairs or carrier-trap pairs is provided by the ε' curves, as shown in Fig. 2.5 . Two peaks are clearly evident; one peak is above the optical gap while the other is below the optical gap. These peaks in the real part of the dielectric constant are directly related to the polarization of the material. The peak of ε' associated with photon energy greater than the band gap is directly related to the

dipole-like behavior of bound electron-hole pairs, while the peak in ε' associated with sub-band gap photon energy is directly related to the dipole-like behavior of bound carrier-trap pairs.

In amorphous materials, one of the most interesting areas is (from both a scientific and practical viewpoint) the energy distribution of the density of states in and around the gap. There is still a great deal of controversy and discussion regarding the density of states; complications arise due to the calculating the density of states in the absence of long range order, assumptions about the matrix elements for optical transitions, difficulty in preparing defect-free material, and other experimental difficulties. Qualitatively, the band tails are created by the absence of long-range order. Superimposed on the density of states diagram are peaks associated with states created by short-range order fluctuations and defects such as dangling bonds. Several investigators [1,49,50] have reported that amorphous Si and Ge films prepared by vacuum deposition or by r.f. sputtering always appear to have a high density of localized states in the gap, in particular at the Fermi level E_f, which is essentially pinned by these gap states. Evidence for the high density of states at E_f is the small value of thermopower, the resistance to doping , and the temperature dependent conductivity, which follows the relation $T^{-1/4}$ derived from hopping conduction at E_f for low temperature. In

these films the highest density of states at E_f is of the order of $10^{18}\,cm^{-3}\,eV^{-1}$, located in energy near midgap. Such a high value of the density of states at E_f has been attributed to dangling bonds and other defects arising from voids in the material. Damage due to ion bombardment in the sputtering environment may also contribute significantly to the high density of defect states.

It is well known that the principal effect of hydrogen incorporated into amorphous Si and Ge is to reduce the density of localized states in the gap [4,51,52]. The reduction in localized states has been attributed to the saturation of dangling bonds with the concomitant removal of states in the gap by hydrogen. It has also been reported [53] that if a:Si(H) prepared by r.f. glow discharge is bombarded by energetic ions, a pronounced $T^{-1/4}$ behavior and a strong ESR signal appear but can be reduced by proper thermal annealing. This clearly indicates that the high density of localized states in the gap is associated with defects such as dangling bonds and voids. The a:$Si_{1-x}\,Ge_x$(H) films used in the present study were fabricated in a gas mixture of Ar and 5% H_2. Although the atomic percent (at%) of the hydrogen concentration in the films was not measured, an estimate was made by comparing our optical bandgap data with data of other workers, for samples having specified hydrogen incorporation [54-56]. From this comparison it is estimated that the hydrogen concentration in the present samples is

about 8 at.%. This hydrogen concentration is relatively small, with the consequence that a large concentration of defects and thus a high density of gap states is expected to exist in these samples.

As has been previously mentioned,the steady-state optical absorption is associated with a large concentration of photogenerated free carriers and with a non-reabsorbing recombination process. However, the refractive index n should be associated with a large concentration of dipole-like bound electron-hole pairs. The high photon energy peak in n as shown in Fig. 2.1 is associated with the maximum concentration of such bound electron-hole pairs which are created by interband transitions under an optimal combination of two processes: the rate of generation of electron-hole pairs, and the number of electron-hole pairs remaining bound without dissociation. The exciting photon energy for the occurrence of this peak is much smaller than the photon energy for the occurance of the peak in ε'' as shown by comparing Figs. 2.1 and 2.6 . This is because the peak associated with n depends on the concentration of electron-hole pairs remaining bound while the peak associated with ε'' depends on the number of avaiable effective transition states. The second peak of n occurs at a photon energy approximatly one-half that of the first peak, i.e. at a photon energy that is less than the optical gap. This implies that the second peak in n is associated with bound electron-hole

pairs in which one carrier is trapped, as created by the transitions to and from gap states.

The question now arises as to the location of these gap states: one possibility is that the highest density of gap states is a band of compensated levels pinning E_f near the middle of the gap as in the Davis-Mott model. Another possibility is that the density of states follows a modified Davis-Mott model, in which case the observation that the photon energy for the second peak in n is approximatly one-half the photon energy for the first peak in n would have been fortuitous. In any case, from Fig 2.1 it can be concluded that a high density of states exists within the mobility gap for all the present a:Si_{1-x} Ge_x (H) samples. The magnitude of the second peak in n is also an indication of the magnitude of the density of gap states.

The present experimental data is believed to be the first set of systematic data on the dispersion of the optical constants of amorphous $Si_{1-x}Ge_x$(H) films with a wide range of composition($0 \leq x \leq 1$), and covering a wide range of wavelengths. The optical band gap E_{opt} varies linearly with alloy composition and is smaller for films prepared by r.f. sputtering than for films prepared by r.f. glow discharge [36] as shown in Fig 2.10 . The lower E_{opt} is thought to be due primarily to the lower hydrogen content in the sputtered films than in the films prepared by glow discharge. The optical band gap in the amorphous phase is nevertheless sig-

nificantly higher than that in the crystalline phase. The observed linear dependence of some parameters upon alloy composition in general is similar to that observed for the alloys in the crystalline phase. This may imply that the short-range order, although extending to only several neighbors, remains a decisive factor in the determination of the gross optical properties of the amorphous material. The use of dispersive data of optical constants can be used for calculations regarding optimum antireflection coatings for photovoltaic applications, as well as extending the study of gap states to other amorphous materials.

Chapter III

ELECTRONIC PROPERTIES OF a:Si_{1-x} Ge_x (H) THIN FILMS

3.1 EXPERIMENTAL TECHNIQUES

The hydrogenated amorphous $Si_{1-x}Ge_x$ alloy films in this study were fabricated in the same laboratory as those of section 2, by r.f. sputtering in an argon-hydrogen gas mixture (in this case 25% H_2). The substrate temperature during deposition was maintained between 220 and 240 ^{0}C, and the amorphous structure was confirmed by means of X-ray diffraction. The germanium concentration was again controlled by varying the total area of silicon segments on a germanium target in a similar manner to the films prepared for the optical measurements. The Ge content was again determined accurately from the X-ray flouresence of the Ge-Kα line. The film thickness was estimated from the surface area, Ge content, Si and Ge densities and the substrate weight before and after deposition.

For the electrical measurements the a:Si_{1-x} Ge_x (H) films were deposited on molybdenum (Mo) films which had been sputtered onto glass substrates. The Mo provided omhic contacts to the back surface. A sandwich structure geometry was employed with semi-transparent evaporated aluminum (Al) electrodes on the top surface. Photoconductivity measurements

were made using phase-sensitive detection techniques; optical illumination from a xenon source was passed through a Bausch-Lomb grating monochromator and was mechanically chopped and simultaneously a reference signal was provided for the lock-in amplifier. This alignment provided an acceptable signal to noise ratio. The samples were mounted on a temperature-controlled probe.

It should be noted that the infrared absorbtion spectrum revealed oxygen as an unavoidable impurity. Another known impurity was argon as detected by secondary X-ray analysis.

3.2 RESULTS AND DISCUSSION

It should be emphasized that the films provided for the electrical measurements contained limited variation between the samples in the Ge content (x). The range of x available for the electrical measurements on the a:Si_{1-x} Ge_x(H) films was $0 \leq x \leq 0.25$.

Figure 3.1 and 3.2 illustrate the dependence of the dark current and the photocurrent upon temperature for several compositions (x). The activation energy for the dark conductivity decreases from approximately 0.96 eV to 0.90 eV as x increases from 0 (a:Si(H)) to 0.25.

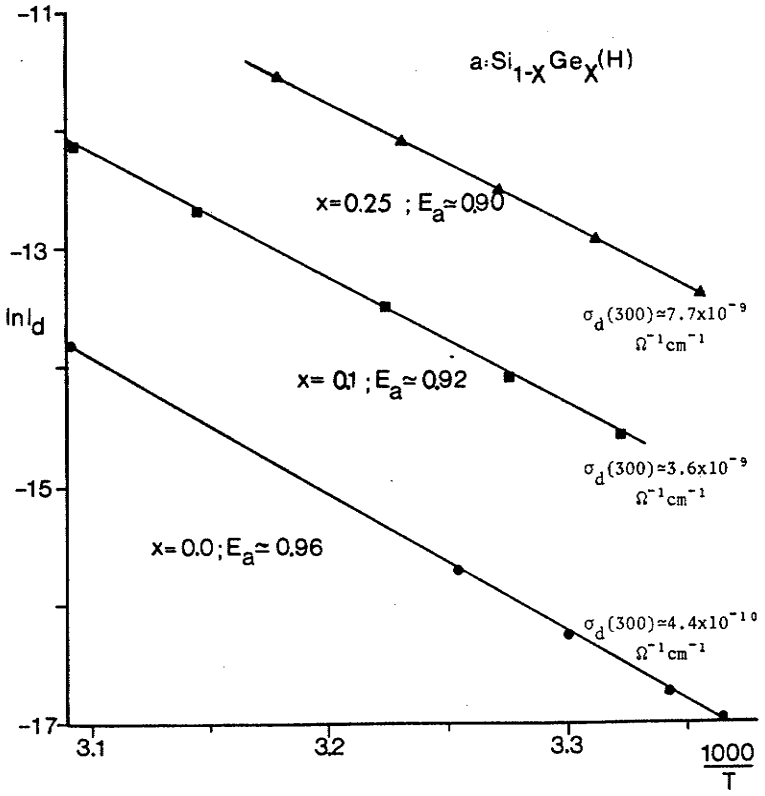

Figure 3.1:Dark current as a function of inverse temperature

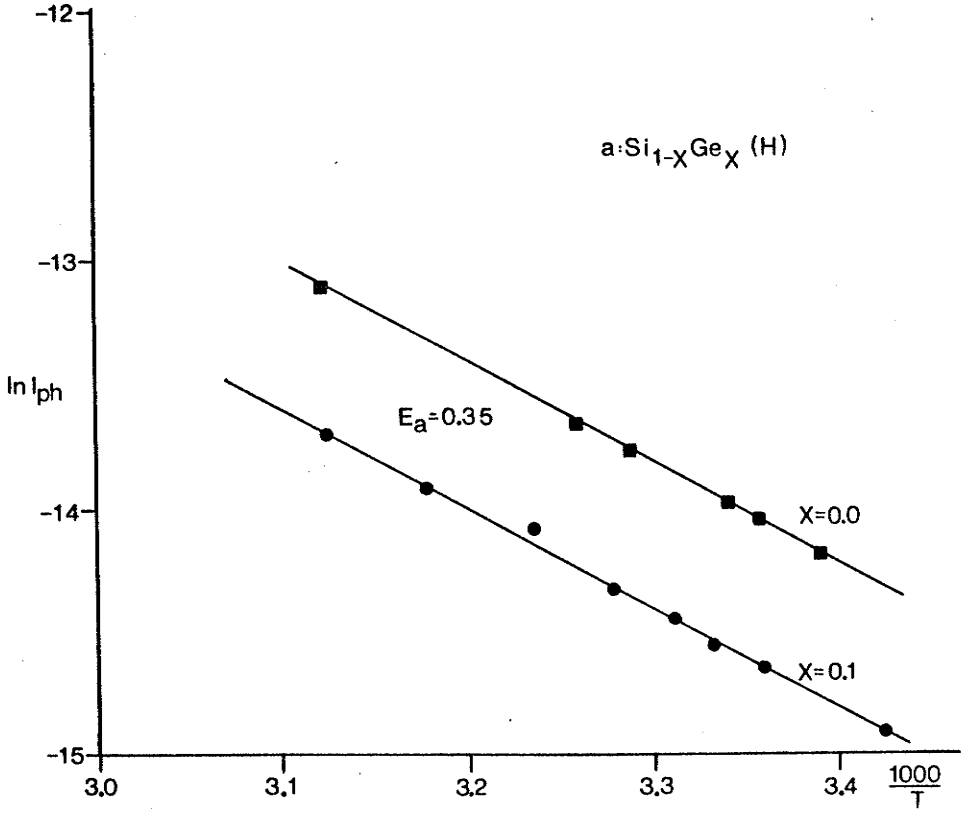

Figure 3.2:Photocurrent as a function of inverse temperature (bimolecular regime)

From the high activation energy for the dark conductivity it may be conjectured that the Fermi level, although pinned, is not at midgap. The Fermi level is more likely pinned at a relatively high density of defect-related localized states below midgap, if we assume predominantly electron conduction. The energy difference between the Fermi level and the conduction band mobility edge is expected to decrease monotonically with increasing Ge content, but the Fermi level is believed to remain below midgap. According to Spear et al. [20-24] conduction at room temperature is by electrons in extended states for glow discharge a:Si(H) films fabricated at a deposition temperature 500 K. In the present study the high values of activation energies associated with the dark conductivities make it difficult to predict unambiguously which type of carrier dominates the conduction. It is plausable to assume that the primary current is due to electron conduction in extended states, while the holes are immobilized by a very high density of defect-related localized states above the valence band mobility edge. The activation energy for the photoconductivity is approximately constant at 0.34 to 0.35 eV for the limited range of compositions studied. The photocurrent measurements were performed under conditions of moderate light intensity in the temperature range where the recombination is bimolecular, with the photocurrent being on the order of the dark current. The high photoconductivity activation energy is believed to be due to

thermally-activated detrapping of carriers from localized defect states approximately 0.35 eV below the conduction band mobility edge (at least for films with low x).

Figure 3.3 shows the dependence of photocurrent upon optical intensity F_o for a:Si(H) under 6328 Å illumination. A transition is observed from monomolecular recombination behavior $I_{ph} \propto F_o$ to bimolecular recombination behavior $I_{ph} \propto F_o^{1/2}$ with increasing intensity [57]. Figure 3.4 demonstrates the approximately linear dependence of the photocurrent upon applied electric field.

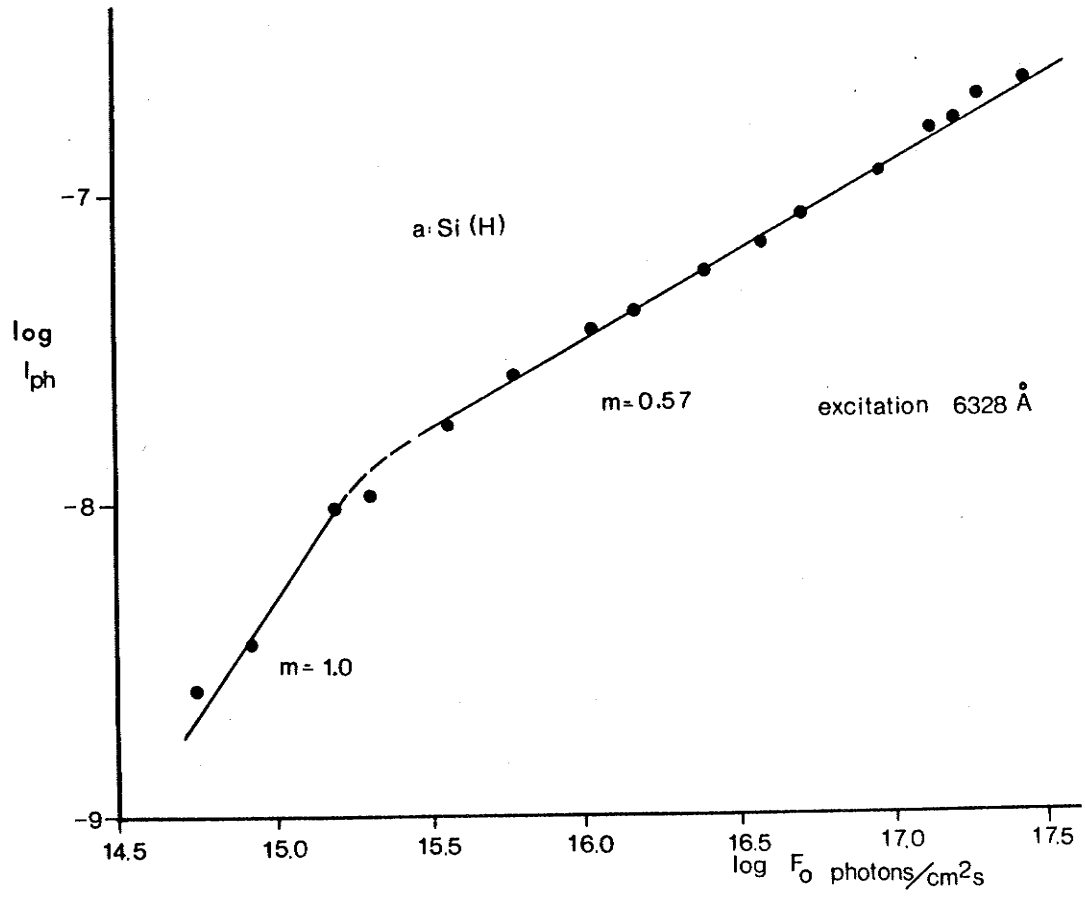

Figure 3.3: Photocurrent versus intensity indicating monomolecular and bimolecular regimes

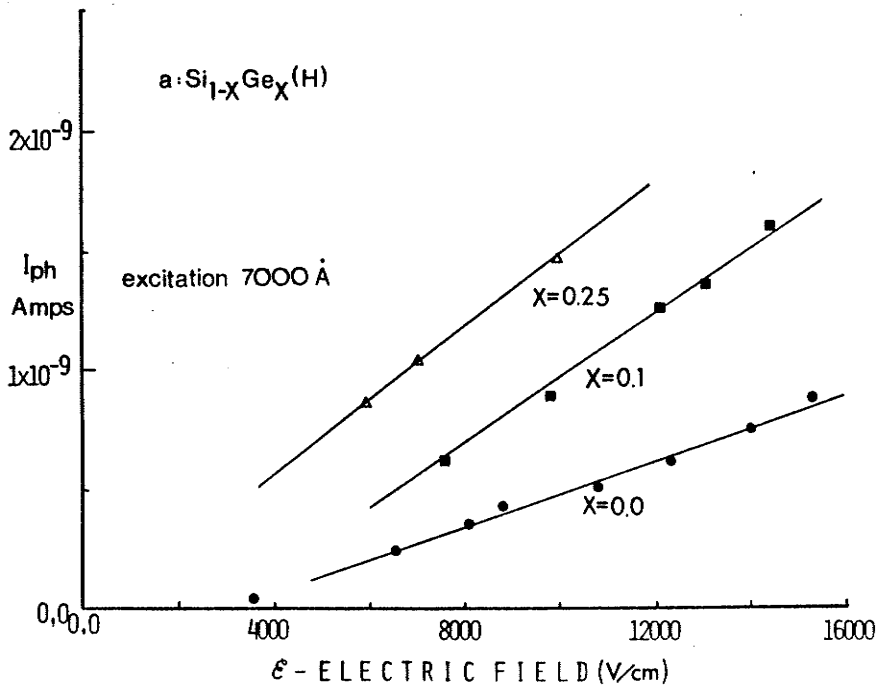

Figure 3.4:Photocurrent versus electric field.

The spectral dependence of the photocurrents on the a:$Si_{1-x}Ge_x$(H) films was measured in the monomolecular recombination region where there is a peak in the photoconductivity versus inverse temperature curves, as shown in Fig. 3.5 [57]. In this region the photocurrent is much less than the dark current. The spectral dependence for the a:$Si_{1-x}Ge_x$(H) films are shown in Fig. 3.6. The reason for the reduction in photocurrent at still higher photon energies is probably surface recombination. Figure 3.6 seems to indicate that a material suitable for amorphous semiconductor solar cells may be one with a small Ge content.

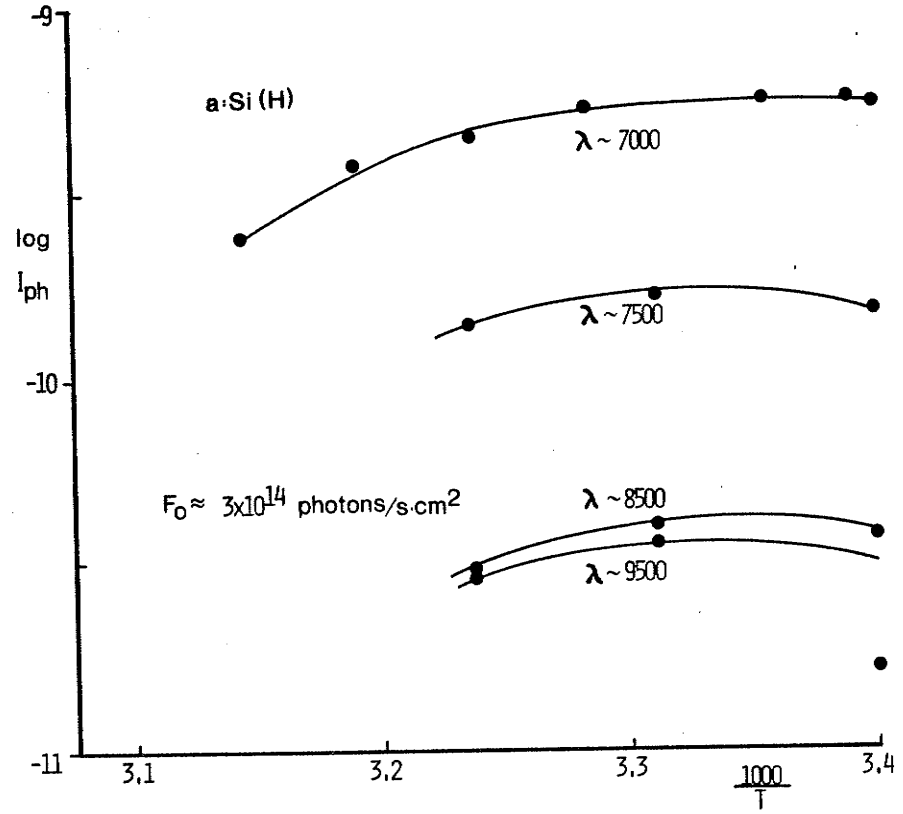

Figure 3.5: Illustration of the range where spectral response measurements were performed.

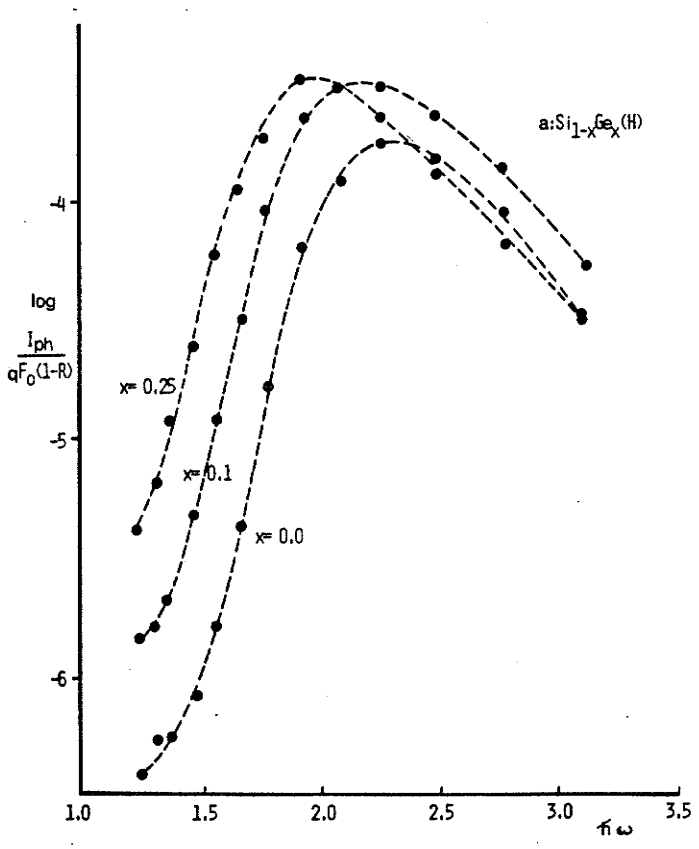

Figure 3.6: Spectral response of a:$Si_{1-x}Ge_x$(H) films

As mentioned earlier, the films prepared for the electrical measurements contain more hydrogen than the films for the optical measurements. This increased hydrogen content is expected to result in a lowering of the density of states within the gap, along with a reduction in the optical absorption coefficient. Following Spear et al. [58] the photocurrent I_{ph} may be described as

$$I_{pH} = eF_o(1 - R)\,[1 - \exp(-\alpha d)]\,\eta\tau/t_d \qquad (3.1)$$

where F_o is the incident photon flux (photons $cm^{-2}\,s^{-1}$) R is the reflection coefficient, η is the internal quantum efficiency, τ/t_d is the ratio of recombination lifetime to transit time and d is the film thickness. In the weakly absorbing region $\alpha d<1$, Eqn. 3.1 reduces to

$$I_{pH} \cong eF_o(1 - R)\alpha d\eta\tau/t_d \qquad (3.2)$$

In Fig. 3.7 $(I_{ph}\hbar\omega/eF_o(1-R))^{1/2}$ versus $\hbar\omega$ is plotted in a similar manner to the earlier discussion of $(\alpha\hbar\omega)^{1/2}$ versus $\hbar\omega$. Provided $\eta\tau/t_d$ is independent of $\hbar\omega$ the intercept in Fig. 3.7 should correspond to E_{opt} , the optical energy gap. The intercepts have been plotted as curve (b) in Fig. 3.8 for comparison with the results from the optical data, curve(a). Considering that the hydrogen content in curve (b) is expected to be somewhat higher than in curve (a), in view of the 25% H_2 as opposed to the 5% H_2 sputtering environments, the comparison is favourable.

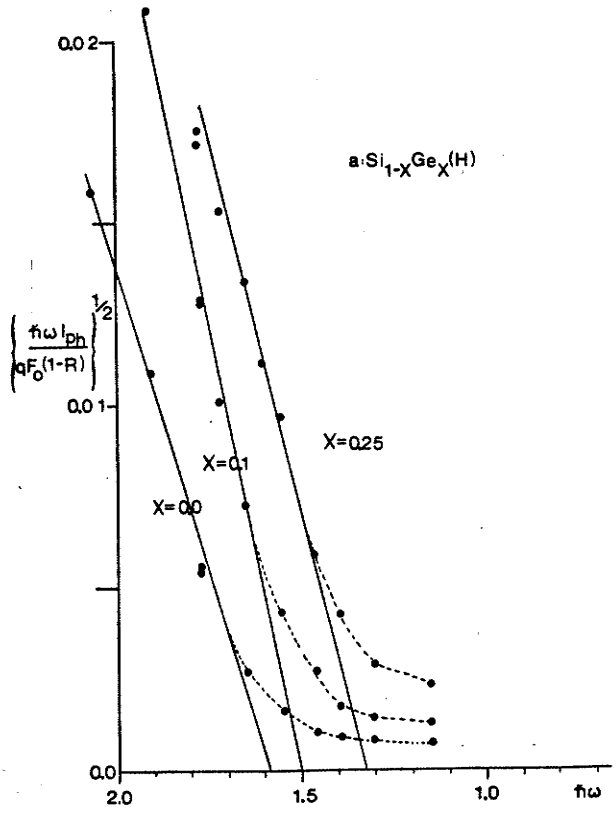

Figure 3.7:Determination of E_{opt} from photoconductivity measurements

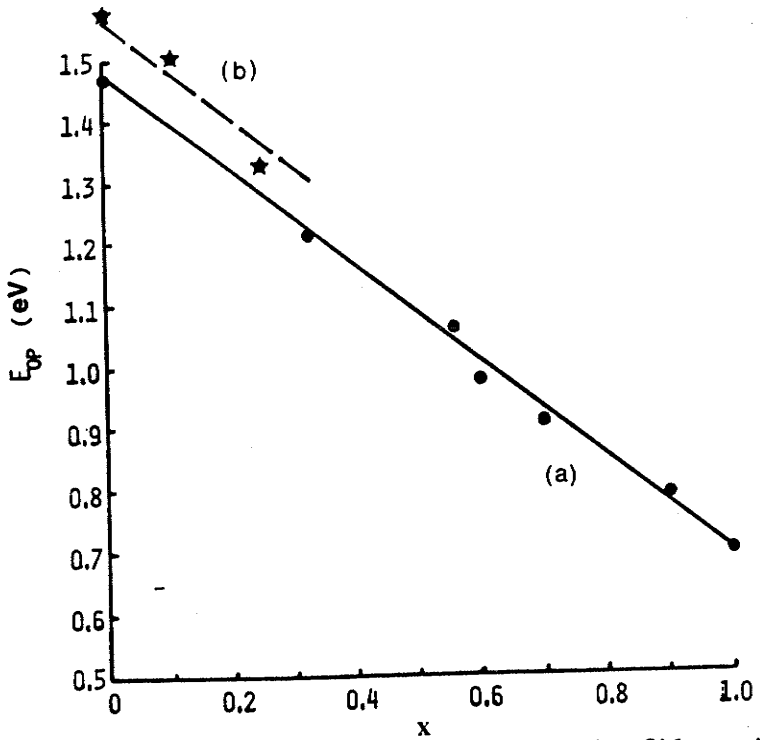

Figure 3.8:Optical band gap of a:$Si_{1-x}Ge_x$(H) thin films. A, E_{opt} derived from the optical measurements (5% H_2 sputtering environment). B, E_{opt} derived from the electrical measurements.

Before leaving the discussion of the electrical properties, it is convenient at this point to clear up any discrepancy that may have arisen due to the assumption of electron conduction in extended states. The high value of activation energy associated with the dark conductivity is not very unusual ; others have reported similar results [22,59,60]. At a first glance the Fermi level appears to be well below midgap requiring a speculative argument to account for the lack of hole current, in view of the apparently larger hole concentration. This claim is nevertheless a reasonable one, provided the electron mobility is substantially larger than the hole mobility, bearing in mind that: 1) The activation energy measured is actually an extrapolated $Ec-E_f$ at 0 K. For amorphous Si, $Ec-E_f$ has been shown [61,62,63] to decrease approximately 0.1 eV as T increases from 0 K to room temperature. This implies that the energy difference $Ec-E_f$ associated with the a:Si(H) sample can be reduced from 0.96 to 0.89 eV; 2) The second factor is that the mobility gap is somewhat larger than the optical gap [63,64]. Assuming, for example a mobility gap of 1.65 eV instead of 1.6 eV (E_{opt}), and using $Ec-E_f \simeq 0.86$ eV, the hole concentration is only 2 orders of magnitude greater than the electron concentration. Under these conditions the argument for electron conduction is favourable, since the hole mobility in the extended states of the valence band is generally considered to be 2 orders of magnitude less than

electron mobility in the extended states of the conduction band. Further immobilization of holes is provided by a high density of traps just above the valence band mobility edge in energy.

Chapter IV

CONCLUSIONS

On the basis of the experimental results regarding the dispersion of the optical constants of the amorphous $Si_{1-x}Ge_x(H)$ films, the following conclusions are drawn:

1) The optical band gap, the peak value of the refractive index, the extinction coefficient and the loss factor at a fixed photon energy, and the photon energy required for a given absorption coefficient, vary monotonically and approximately linearly with the Ge content in the a:$Si_{1-x}Ge_x(H)$ films. 2) In the low Ge content films there exist two peaks in the spectra of the refractive index and indications of two peaks in the spectra of the extinction coefficient. The first peak is associated with interband transitions, and the second peak with the transitions to and from localized states within the mobility gap. 3) The photon energy for the occurrence of the peak value of ε'', termed E_{PH}, is close to the energy for the maximum rate of change of the effective states available for optical transitions. E_{PH} is larger than the so-called optical band gap E_{opt}. 4) The peak of the refractive index is associated with the maximum density of (dipole-like) bound electron-hole

pairs, generated by optical transitions and remaining thermally undissociated.

From the experimental results of the electrical measurements on the a:$Si_{1-x}Ge_x$(H) films ($0 \leq x \leq 0.25$) the following conclusions are proposed:

1) The Fermi level may be pinned by defect-related states at an energy slightly below midgap. This is evidenced by the large activation energy for dark conductivity. 2) Assuming primarily electron conduction in extended states, the activation energy associated with the photoconductivity is attributed to thermally-activated detrapping of carriers from localized defect states below Ec.

On the basis of the combined optical and electrical results, the following model of r.f. sputtered amorphous $Si_{1-x}Ge_x$(H) thin films is advanced:

To begin with, optical and electronic measurements are all consistent with the general features of a modified Davis-Mott model, such as that of Fig. 4.1 . From the activation energy for the dark conductivity $E_c - E_f \simeq 0.96$ eV for a:Si(H), and the value of the corresponding optical gap $E_{opt} \simeq 1.6$ eV, we can further deduce that the equilibrium Fer-

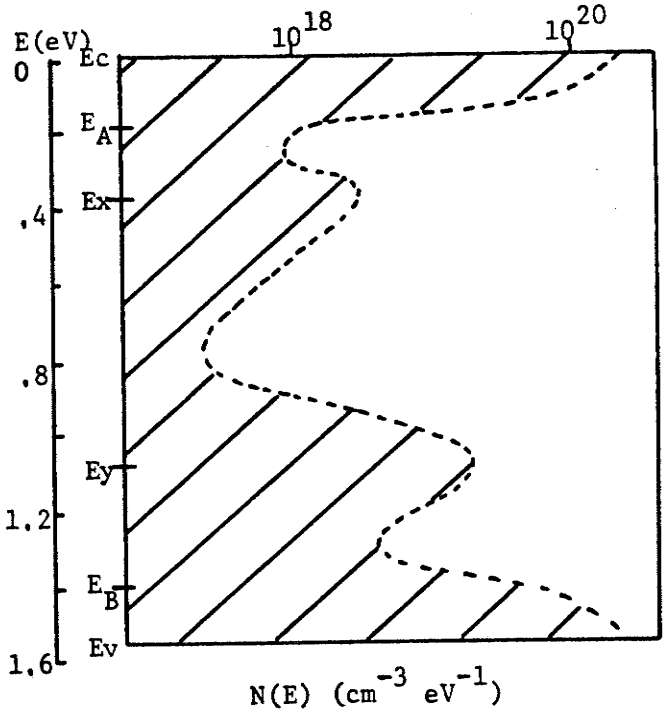

Figure 4.1:Approximate density of states distribution for sputtered a:Si(H), following that proposed by Spear et al. [20-24] for glow discharge produced a:Si(H).

mi level is pinned below midgap. This remains true as x increases. This interpretation is corroborated by the transition from monomolecular to bimolecular recombination with increasing optical intensity (transition from low-level to high-level injection as expected for an equilibrium Fermi level energetically located away from midgap). Assuming primarily electron conduction in extended states (near room temperature) the activation energy associated with the photoconductivity is interpreted as a determination of Ec-Ex as shown in Fig. 4.1 . Photogenerated electrons become trapped at Ex and must be thermally excited to Ec to contribute to the conduction. Ec-Ex remains approximately independent of

x for small x. Finally, hole mobilities are well below those of electrons (by at least 2 orders of magnitude) since their activation energy is somewhat smaller, and yet they appear not to contribute to the conduction in these materials. The holes may of course also be immobilized by trapping at a high density of defect-related (localized) states above the valence band mobility edge at Ey as shown in Fig. 4.1 . The form of the density of states presented here is reminescent of earlier results for a:Si(H) thin films produced by glow discharge techniques [20-24].

REFERENCES

1) N.F. Mott and E.A. Davis, Electronic Processes in Non-Crystalline Materials, Second Edition (Clarendon, Oxford, 1979).

2) M.H. Brodsky (Editor), Amorphous Semiconductors, (Springer-Verlag,New York, 1979).

3) S.K. Bahl and S.M. Bhagat, J. Non-Cryst. Solids 17, 409 (1975).

4) G.A.N. Connell and J.R. Pawlik, Phys. Rev. B13, 787 (1976).

5) D.K. Paul and S.S. Mitra, J. Non-Cryst. Solids 18, 407 (1975).

6) S. Hasegawa, S. Yazaki, and T. Shimizu, Solid State Communications 26, 407 (1978).

7) W.P. Spear, Advances in Phys. 26, 811 (1977).

8) W.P. Spear and P.G. Lecomber, Phil. Mag. 33, 935 (1976).

9) T.S. Nashashibi, I.G. Austin and T.M. Searle, Phil. Mag. 35, 831 (1977).

10) E.C. Freeman and W. Paul, Phys. Rev. B20, 716, (1979).

11) W. E. Spicer and T. M. Donoven, J. Non-Cryst. Solids 2, 66, (1970).

12) M.H. Brodsky, R.S. Title, K. Weiser, and G.D. Pettit, Phys. Rev. B1, 2632 (1970).

13) A.J. Lewis, Phys. Rev. B14, 658, (1976).

14) N.V. Dong, T.H. Danh and J.Y. Leny, J. Appl. Phys. 52, 338, (1981).

15) D. Beaglehole and M. Zavetova, J. Non-Cryst. Solids 4, 272 (1970).

16) J. Chevallier, H. Wieder, A. Onton, and C.R. Guarniert, Solid State Communications 24, 867 (1977).

17) G.A.N. Connell, in Amorphous Semiconductors (ed. by M.H. Brodsky, Springer Verlag, New York, 1979), p. 73.

18) P. W. Anderson, Phys. Rev. 109, 1942 (1958).

19) M.H. Cohen, H. Fritzsche and S.R. Ovshinsky, Phys. Rev. Lett. 22, 1065 (1969).

20) W.E. Spear, P.G. Lecomber, J. Non-Cryst. Solids 8-10, 727 (1972).

21) P.G. Lecomber, A. Madan and W. E. Spear, J.Non-Cryst. Solids 11, 219 (1972).

22) R.J. Loveland, W.E. Spear, and Al-Sharbaty, J. Non-Cryst. Solids 13, 55 (1973/74).

23) W.E. Spear, R.J. Loveland and Al-Sharbaty, J. Non-Cryst. Solids 15, 410 (1974).

24) A. Madan, P.G. LeComber and W.E. Spear, J. Non-Cryst. Solids 20, 239 (1976).

25) P. Nagels, in Amorphous Semiconductors (ed. by M.H. Brodsky, Springer Verlag, New York, 1979), p. 73.

26) N.F. Mott, in Electronic and Structural Properties of Amorphous Semiconductors (ed. by P.G. Lecomber and J. Mort, Academic Press, New York, 1973), p. 1.

27) M.H. Cohen, J. Non-Cryst. Solids 4, 391 (1970).

28) A.J. Grant and E.A. Davis, Solid State Comm. 15, 563 (1974).

29) A. Rose, RCA Rev. Sept. 362 (1951).

30) J.E. Fischer and T.M. Donovan, J. Non-Cryst. Solids 8-10, 202 (1972).

31) P.J. Zanzucchi, C.R. Wronski, and D.E. Carlson, J. Appl. Phys. 48, 12 (1977).

32) J.G. Simmons and G.W. Taylor, J. Non-Cryst. Solids 8-10, 947 (1972).

33) J.G. Simmons, G.W. Taylor, J. Phys. C: Solid State Phys. 7, 3067 (1974).

34) D.L. Staebler, C.R. Wronski, J. Appl. Phys. 51, 3262 (1980).

35) P.E. Vanier, A.E. Delahoy, and R.W. Griffith, J. Appl. Phys. 52, 5235 (1981).

36) N.F. Mott, E.A. Davis, Philos. Mag. 32, 961 (1975).

37) N.K. Hindley, J. Non-Cryst. Solids 5, 17 (1970).

38) G.A.N. Connell, W. Paul and R.J. Temkin, in Amorphous and Liquid Semiconductors, (ed. by J. Stuke, W. Brenig, Wiley, New York, 1974), p. 541.

39) W.E. Spicer, T.M. Donovan, J. Non-Cryst. Solids 2, 66 (1970).

40) G.A.N. Connell and A. Lewis, Phys. Stat. Sol. 60, 291 (1973).

41) H. Watanabe and K.C. Kao, J. of Vacuum Society of Japan 24, 417 (1981).

42) H. Watanabe and K.C. Kao, Japanese J. Appl. Phys. 20, 789 (1981).

43) H. Adachi and K.C. Kao, J. Appl. Phys. 51, 6326 (1980).

44) E.L. McCracken, A Fortran Program for Analysis of Ellipsometer Measurement (Nat. Bur. Stand., Washington, D.C., 1969) Technical Note 479.

45) K.C. Kao, R.D. McLeod C.H. Leung, H.C. Card and H. Watanabe "submitted for publication".

46) J. Tauc, in Amorphous and Liquid Semiconductors, (ed. by J. Tauc, Plenum, New York, 1974).

47) W.C. Dash and R. Newman, Phys. Rev. 99, 1151 (1955).

48) R. Braunstein, A.R. Moore and F. Herman, Phys. Rev. 100, 695 (1958).

49) H. Mell, in Proc. 5th Int. Conf. Amorphous and Liquid Semiconductors (ed. by J. Stuke, and W. Brenig, Taylor and Francis, London, 1974), p. 203.

50) E.A. Davis, in Amorphous Semiconductors (ed. by M.H. Brodsky, SpringerVerlag, New York, 1979), p. 41.

51) A.J. Lewis, G.A.N. Connell, W. Paul, J.R. Pawlik, and R.J. Temkin in Proceedings of the International Conference on Tetrahedrally Bonded Amorphous Semiconductors, edited by M.H. Brodsky, S. Kirkpatrick and D. Weaive (American Institute of Physics, New York 1974), p. 27.

52) T.D. Moustakas and W. Paul, Phys. Rev. B16, 1564 (1977).

53) J. Stuke, "Structure and properties of non-crystalline semiconductors", in Proc. 6th Int. Conf. Amorphous and Liquid Semiconductors, edited by B.T. Kolomiets, (Academy of Sciences of USSR, Nauka, 1976), p. 193.

54) P.M. Martin and W.T. Pawlewicz, Solar Energy Materials 2, 143 (Dec. 1979 - Mar. 1980).

55) F.R. Jeffrey, H.R. Shanks and G.C. Danielson, J. Non-Cryst. Solids 35-36, 261 (1980).

56) H. Okzmoto, T. Yamaguchi, Y. Nitta, and Y. Hamakawa, J. Non-Cryst. Solids 35-36, 201 (1980).

57) N.F. Mott, E.A. Davis and R.A. Street, Phil. Mag. 32, 961 (1975).

58) W.E. Spear and P.G. Lecomber, in Photoconductivity and Related Phenomena, (ed. by J. Mort and D.M. Pai, Elsevier, New York, 1976).

59) N.B. Goodman, H. Fritzsche and H. Ozaki, J. Non-Cryst. Solids 35 & 36, 599 (1980).

60) P.E. Vanier and R.W. Griffith, J. Appl. Phys. 53, 3098 (1982).

61) H. Fritzsche, in Electronic and Structural Properties of Amorphous Semiconductors , (ed. by P.G. Lecomber and J. Mort, Academic Press, New York, 1973), p. 55.

62) J. Perrin and I. Solomon, J. Non-Cryst. Solids 37, 407 (1980).

63) R.W. Griffith, J. Non-Cryst. Solids 24, 413 (1977).

64) E.A. Davis and R.F. Shaw, J. Non-Cryst. Solids 2, 406 (1970).

65) G.A.N. Connell, R.J. Temkin and W. Paul, Adv. Phys. 22, 643 (1973).